Punching of reinforced concrete slab without shear reinforcement: standard models and new proposal

Luisa Pani[1], Flavio Stochino[2]*

[1]Department of Civil, Environmental Engineering and Architecture, University of Cagliari (Italy).

lpani@unica.it – ORCID 0000-0003-4811-2506

[2]Department of Civil, Environmental Engineering and Architecture, University of Cagliari (Italy).

* Corresponding author, fstochino@unica.it – ORCID 0000-0002-0786-9070

Abstract

Reinforced concrete (RC) slabs are characterised by reduced construction time, versatility, and easier space partitioning. Their structural behaviour is not straightforward and, specifically, punching shear strength is a current research topic.

In this study an experimental database of 113 RC slabs without shear reinforcement under punching loads was compiled using data available in the literature. A sensitivity analysis of the parameters involved in the punching shear strength assessment was conducted, which highlighted the importance of the flexural reinforcement that are not typically considered for punching shear strength.

After a discussion of the current international standards, a new proposed model for punching shear strength and rotation of RC slabs without shear reinforcement was discussed. It was based on a simplified load-rotation curve and new failure criteria that takes into account the flexural reinforcement effects.

This experimental database was used to validate the approaches of the current international standards as well as the new proposed model. The latter proved to be a potentially useful design tool.

Keywords: Punching shear strength, reinforced concrete, slabs, reinforcement ratio.

Please cite this document as: Pani, L., Stochino, F. Punching of reinforced concrete slab without shear reinforcement: Standard models and new proposal. *Front. Struct. Civ. Eng.* (2020). https://doi.org/10.1007/s11709-020-0662-z

1. Introduction

The use of reinforced concrete (RC) slabs has a number of advantages, including reduced and simpler formwork, versatility, and easier space partitioning. They represent economical and efficient structural systems, but however common their use may be, their structural behaviour is not straightforward and has been analysed over numerous years [1]. It is the subject of current studies that are considering its response under impulsive and blast loading [2]-[5].

Therefore, the analysis of punching in RC slab is topical for a number of reasons. Punching collapse can be dangerous as it develops with a brittle mechanism and affects the integrity of the structure. A localised punching collapse can result in a general structural failure. A very interesting state of the art report is presented in [6].

International standards (Eurocode 2 [7], ACI 318 [8], and Model Code 2010 [9]) present different punching models and prescriptions that yield different structural design results. In addition, if a comparison between theoretical and experimental punching shear strengths [10] - [20] is conducted, different safety coefficients are obtained.

In Model Code 2010 (MC10) [9] the punching shear strength model is based on the critical shear crack theory (CSCT) [21], whereas ACI 318 [8] and Eurocode 2 (EC2) [7] refer to empirical models based on the maximum shear stress. The CSCT also provides an estimate of the slab rotation from punching; however, the other two models do not provide this information.

Comparisons between the theoretical models and the experimental results can be found in the literature (see [11],[13],[19],[20] and [22]-[24]), but they either do not consider all of the standard models or their experimental benchmark databases are limited. Siegrist et al. [25] point out that shear resistance understanding is incomplete and provide a very interesting discussion on the advantage of physical models over empirical formulae.

Over the past few years, a number of researchers have analysed the effects of fibre reinforcement on RC structures and on RC slabs subject to punching loads [26] - [28] with the aim of assessing the performance of new materials and innovative technologies. In particular, [27] presents an innovative

Please cite this document as: Pani, L., Stochino, F. Punching of reinforced concrete slab without shear reinforcement: Standard models and new proposal. *Front. Struct. Civ. Eng.* (2020). https://doi.org/10.1007/s11709-020-0662-z

approach for the design of punching shear reinforcement for RC slabs using fibre reinforced polymer bars and stirrups. An interesting experimental analysis is developed in [28] where the punching performance of RC slabs strengthened with ultra-high performance fibre reinforced cement-based composite is described.

Interesting results were obtained with reinforced recycled concrete slabs ([14]-[15],[18], and [29]-[32]), where the low mechanical performance of the materials corresponded to unexpectedly good structural performance of the whole structural element. For example in [14] is shown as the increasing replacement percentage of recycled aggregates with respect to the natural ones produced a reduction of compressive strength and elastic modulus of concrete, but RC slab specimens realized with recycled aggregates present the same punching resistance of slab realized with natural aggregates.

Concrete elements with plastic void formers [33] and lightweight aggregate were also tested for punching shear strength, and [34] reports on both experimental results and design equations considering slabs with small reinforcement ratios.

In RC slabs without shear reinforcement (see [34] - [35]), brittle punching failure may be a critical factor in the design, and specific attention should be paid to this to ensure adequate deformation and redistribution of bending moments.

The empirical approach, adopted in a number of international codes, is sufficient for simple design practice. In addition, further limitations in construction details lead to very conservative approaches. However, to develop efficient construction systems, it is essential to understand the physical phenomena and to justify the behaviour of existing slabs whenever they do not fall within the typical limits and conditions.

In this study the punching shear strength models adopted by the abovementioned international standards (ACI 318, EC2, and MC10) are discussed in Section 2 in order to highlight the characteristics, limits, and reliability of each model. A comprehensive experimental database was developed using the results reported in the literature, and direct comparisons with the theoretical models, and their analysis are presented in Section 3. The considered database is representative of the entire population of RC slabs under punching load, as the frequency distribution of the key parameters considered in the theoretical

models is sufficiently uniform. A sensitivity analysis is developed and is explained in Section 4; this analysis identifies the primary geometric and mechanical parameters which influence the experimental punching shear strength. The proposal of a new punching shear strength model based on CSCT is presented in Section 5. This model takes into account the rotation capacity of the slab and it is designed specifically for elements without shear reinforcement. It is characterized by a parameter representing the flexural reinforcement in the collapse criterion formulation. Thus, it can highlight the flexural reinforcements role in RC slab punching. The conclusions drawn are presented in Section 6.

2. Standard theoretical models for punching shear strength

2.1 ACI 318

The model presented in ACI 318 [8] assesses the punching shear strength of slabs without specific shear reinforcement but does not provide any information regarding their rotation capability. In this case, the punching load $V_{theo,ACI}$ (N) is obtained as the minimum value between equations (1.a, 1.b, and 1.c).

$$V_c = 0.17 \cdot \left(1 + \frac{2}{\beta}\right) \cdot \lambda \cdot \sqrt{f_c} \cdot b_0 \cdot d \quad (1.a)$$

$$V_c = 0.083 \cdot \left(\frac{\alpha_s \cdot d}{b_0} + 2\right) \cdot \lambda \cdot \sqrt{f_c} \cdot b_0 \cdot d \quad (1.b)$$

$$V_c = 0.33 \cdot \lambda \cdot \sqrt{f_c} \cdot b_0 \cdot d \quad (1.c)$$

where β is the ratio between the minimum and maximum dimensions of column cross sections (or loading surface); α_s=40 for an interior column, 30 for a side column, and 20 for a corner column; λ=1 for normal weight concrete and 0.75 for lightweight concrete, and is determined considering volumetric proportions of lightweight and normal weight[1] aggregates (see §8.6 ACI 318 [8]); f_c (MPa) is the cylindrical compressive strength of concrete, b_0 (mm) is the perimeter of the critical section located at a distance *d/2* from the edges of the loaded area (in the critical section curved corners are not taken into

[1]According to ACI 318 [8]normal weight concretes are characterised by a density varying between 2155–2560 kg/m^3.

consideration); and *d* (mm) is the effective depth (the distance from extreme compression fibre to the centroid of the longitudinal flexural reinforcement of the cross section), see Figure 1.

This model does not consider the contribution of flexural reinforcement to punching shear strength, which is typically determined by equation (1.c). However, experimental tests have shown that thin slabs [10] and elongated rectangular load areas [12] exhibit significant resistance reductions, and that equation (1.c) is not conservative. Specifically, if the greatest load surface size is considerably greater than the thickness of the slab, the appropriate equations are (1.a) and (1.b). In addition, for square columns, equation (1.b) is valid when the side of the load surface is approximately four times greater than the thickness of the slab. In the case of significantly elongated rectangular load surfaces (height/base ratio > 3), the experimental results indicate that the optimum equation to be used is (1.a).

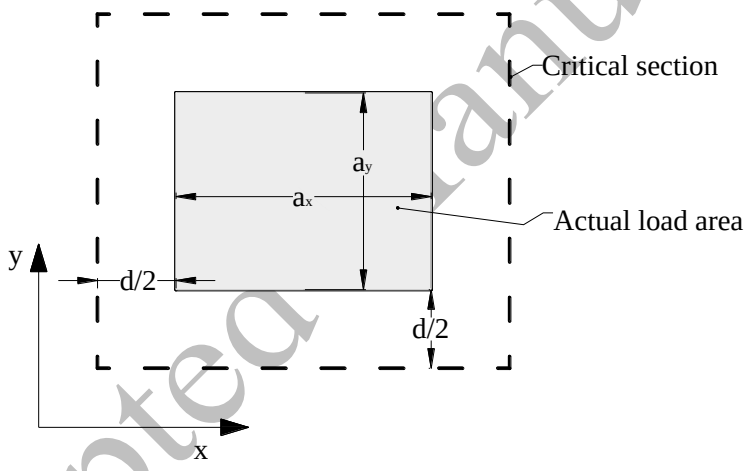

Fig. 1: ACI 318 critical perimeter.

The ACI 318 punching model can be beneficial to the early design of slab dimensions, as it allows determination of the slab thickness knowing the punching load, surface load, and concrete mechanical characteristics.

2.2 Eurocode 2

The Eurocode 2 (EC2) [7] punching model is capable of assessing the punching shear strength of slabs without shear reinforcement, but does not provide any information concerning rotation capability. The theoretical punching strength $V_{theo,EC2}$ is given by equation (2).

$$V_{theo,EC2} = \left[\frac{0.18}{\gamma c} k \cdot (\rho_1 100\, f_{ck})^{\frac{1}{3}} + k_1 \sigma_{cp}\right] \cdot b_0 d \geq \left(v_{min} + k_1 \sigma_{cp}\right) \cdot b_0 d \quad (2)$$

where γ_c = 1.5; $k = 1 + \sqrt{\frac{200}{d}} \leq 2.00$, d in mm; $\rho_l = \sqrt{\rho_{lx} \cdot \rho_{ly}} \leq 0.02$; ρ_{lx} and ρ_{ly} are the reinforcement ratios of the flexural reinforcement in the x- and y-directions, respectively; $v_{min} = 0.035 \cdot k^{3/2} \cdot f_{ck}^{1/2}$; σ_{cp} represents the prestressing stress, k_1=0.1; and b_0 is the perimeter of the critical section, as can be seen in Figure 2.

The EC2 allows the determination of the slab thickness given the surface load sizes, concrete compressive strength, and reinforcement ratio. However, these parameters can be unknown in the early stages of structural design.

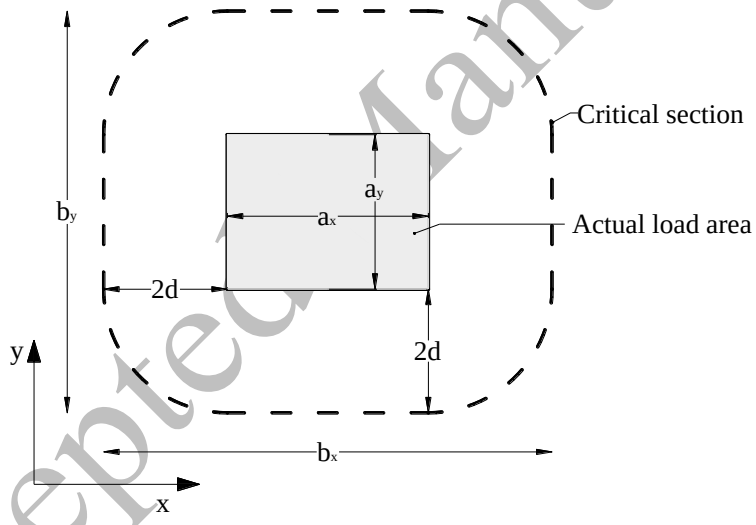

Fig. 2: EC2 critical perimeter for rectangular column.

2.3 Model Code 2010

According to MC10 [9], the theoretical punching shear strength and the corresponding rotation of the slab can be determined by the intersection of the load-rotation curve and the punching failure criterion.

The MC10 load-rotation curve representing the flexural behaviour of the slab without shear reinforcement is based on the CSCT proposed by Muttoni [21] on the base of the works carried out in Switzerland in the 80s.

Actually, MC10 provides four different approximation levels (from I to IV) to estimate the rotation ψ. In this work the authors consider MC10 level II approach that is more accurate than level I without the computational cost of the nonlinear analysis required in the level IV case. Finally, level III is recommended for irregular slabs with particular geometric characteristics.

The MC10 level II approach is based on a re-distribution of the bending action expressed by the following equation:

$$\psi = 1.5\frac{r_s}{d}\cdot\frac{f_y}{E_s}\cdot\left(\frac{m_{Ed}}{m_{Rd}}\right)^{1.5} \quad (3)$$

where E_s is the steel elastic modulus (typically 200 GPa); f_y is the steel yielding strength; r_s can be expressed as $0.22\cdot L_x$ and $0.22\cdot L_y$ for the *x*- and *y*-directions, respectively, in the case of regular slab with span ratios (L_x/L_y) ranging from 0.5–2; m_{Ed} is the bending moment from loads per unit length used for reinforcement design in a given direction; m_{Rd} is the bending moment capacity per unit length for a given direction. In evaluating m_{Rd}, the following assumptions are made: plane sections remain plane; the strain in bonded reinforcement, whether under tension or compression, is the same as that in the surrounding concrete; the tensile strength of the concrete is ignored; stress block distribution is as for concrete under compression; and perfect elastic-plastic behaviour for steel reinforcement under tension and compression.

The collapse scenario hypotheses are as follows: concrete ultimate compressive strain equal to 3.5‰; and yielded flexural steel reinforcement. The compressive reinforcement is not taken into account.

$$m_{Rd} = \rho\cdot d^2\cdot f_y\cdot\left(1-\frac{\rho\cdot f_y}{2\cdot f_c}\right) \quad (4)$$

where ρ is the tensile reinforcement ratio; and, f_c is the concrete compressive strength.

For internal columns without eccentricity of shear-force V_{Ed}, it is typically taken such that $m_{Ed} = V_{Ed}/8$. Therefore, considering equations (3) and (4), it is possible to obtain a simplified load-rotation equation:

$$V = 8 \cdot m_{Rd} \cdot \left[\frac{\psi \cdot E_s \cdot d}{1.5 \cdot r_s \cdot f_y}\right]^{2/3} \quad (5)$$

The intersection between the load-rotation equation (5) and the failure criterion equation (6) provides the theoretical punching shear load.

$$V_{R,punch} = k_\psi \cdot \frac{\sqrt{f_c}}{\gamma_c} \cdot b_0 \cdot d \quad (6)$$

where d is the effective depth of the slab; b_0 is the critical perimeter at a distance $d/2$ from the actual load area; and the parameter k_ψ is related to the slab rotation ψ by the following equation:

$$k_\psi = \frac{1}{1.5 + 0.9 \cdot k_{dg} \cdot \psi \cdot d} \leq 0.6 \quad (7)$$

If the aggregate maximum size is greater than 16 mm, then $k_{dg} = 1$, and if it is smaller than 16 mm,

$$k_{dg} = \frac{32}{16 + d_g} \geq 0.75 \quad (8)$$

For high-strength concrete lightweight concrete, the aggregate particles could break, resulting in a reduced aggregate interlock contribution. Therefore, it is conservative to assume $k_{dg} = 2$ (in which case, $d_g = 0$).

Figure 3 shows the load-rotation and failure criterion curves. The intersection point is highlighted, and represents the theoretical punching load $V_{theo,\,MC10}$ and the corresponding rotation $\psi_{theo,\,MC10}$.

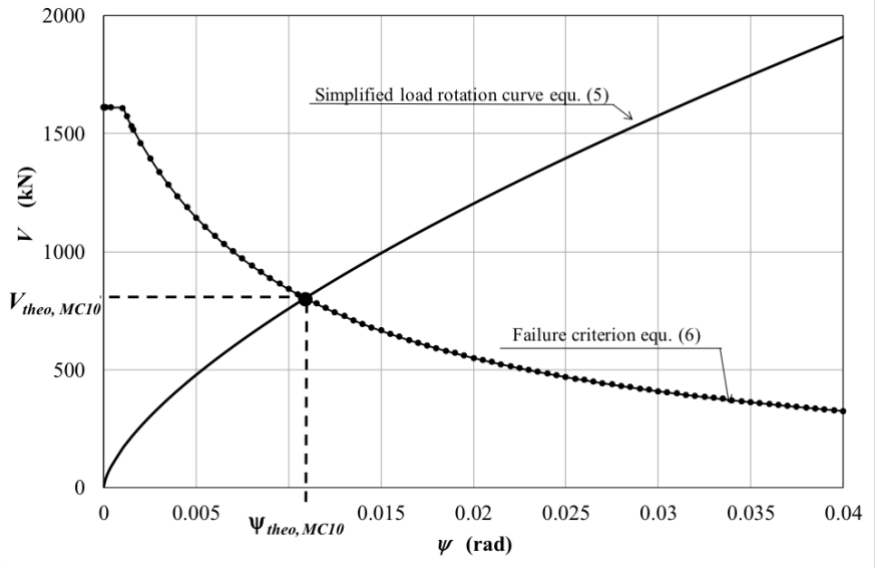

Fig. 3: Load-rotation curve for reinforced concrete slab (equation 5), failure criterion curve (equation 6) and intersection point representing theoretical punching load $V_{theo,MC10}$ and relative theoretical rotation $\psi_{theo,MC10}$.

The exact punching strength can be obtained from the MC10 model using a numerical iterative process to determine the intersection point ($\psi_{theo,MC10}$, $V_{theo,MC10}$) of equations (5) and (6). If $V_{theo,MC10}$ is smaller than V_{Ed} the slab characteristics must be modified. However, a simple design check can be performed calculating the slab rotation ψ_d corresponding to the shear force V_d using equation (5). Then, the corresponding punching shear strength can be obtained plugging ψ_d in the failure criterion (equation (6)), see Figure 14 in [21].

2.4 Standard models discussion

The three models (ACI 318, EC2, and MC10) are currently the predominant models available for punching load assessment.

ACI 318 is based on a purely empirical model and does not consider the contribution of the flexural reinforcement. EC2 is based on the comb model integrated and tuned by several experimental parameters.

The MC10 model is based on CSCT, as above mentioned. It is notable that its load-rotation curve (equation (5)) depends on the flexural reinforcement, while the failure criterion equation (6) does not consider this parameter. In contrast with the ACI 318 and EC2 models, but in agreement with Walraven [36], Vecchio and Collins [37], and Muttoni [21], the MC10 punching shear model considers a direct relationship between the punching shear strength and the maximum aggregate size. The roughness of the critical crack and its capacity to resist shear forces is proportional to the maximum aggregate size. Also, other recent studies addressed the influence of the maximum aggregate size to the shear strength: see [38] - [40].

It is of interest to develop a reliability analysis based on experimental data which can be found in literature using the abovementioned models. In this manner it is possible to assess and compare their performance in punching shear strength evaluation for RC slabs without shear reinforcement.

Please cite this document as: Pani, L., Stochino, F. Punching of reinforced concrete slab without shear reinforcement: Standard models and new proposal. *Front. Struct. Civ. Eng.* (2020). https://doi.org/10.1007/s11709-020-0662-z

Please cite this document as: Pani, L., Stochino, F. Punching of reinforced concrete slab without shear reinforcement: Standard models and new proposal. *Front. Struct. Civ. Eng.* (2020). https://doi.org/10.1007/s11709-020-0662-z

3. Experimental database

From a literature search the authors developed a database of 113 experimental punching test results. The rectangular or circular RC slabs are simply supported along the edges, do not have specific shear reinforcement, and are characterised by slenderness, reinforcement ratio, concrete strength, and maximum aggregate size varying over a wide range in order to represent the bulk of actual cases.

Figure 4 presents the experimental punching load and rotation $(V\text{-}\psi)_{punch,exp}$ data gathered from the literature. In addition, in Table 1 the reference, sample number, publication year, primary focus of the research, and the method used to assess the punching rotation of database are presented. The $\psi_{punch,exp}$ was directly assessed in a number of cases and obtained by indirect measurement, and as the ratio between the deflection and the span length in other cases (Table 1: *D* = direct measurement; and *I* = indirect measurement).

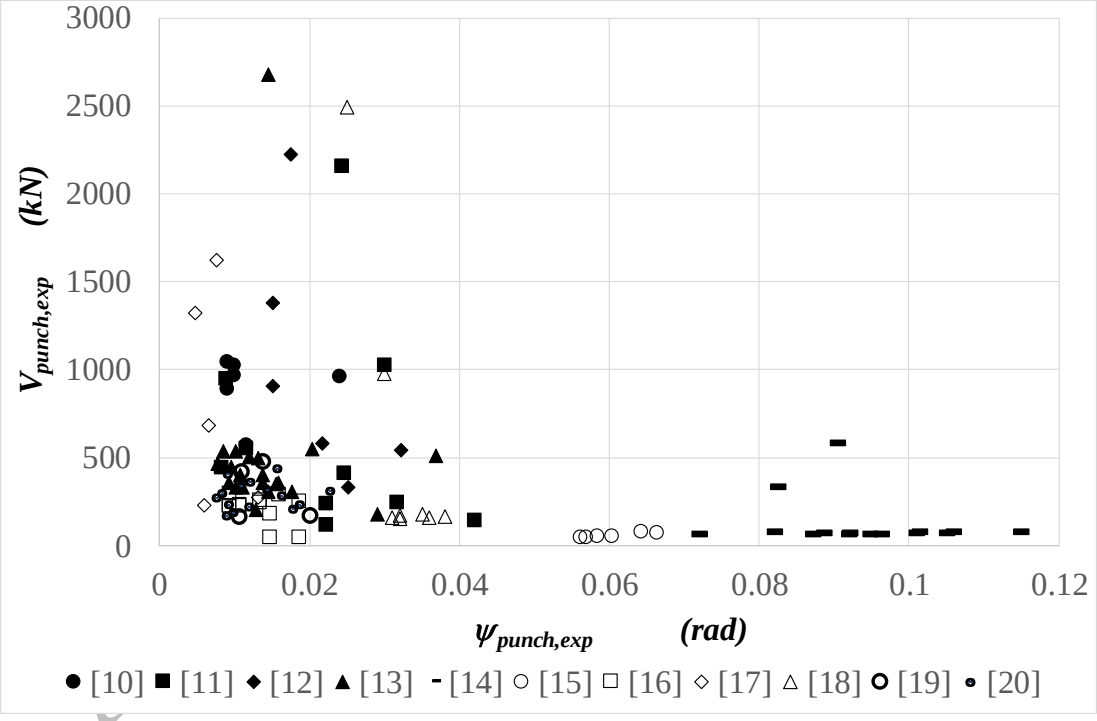

Fig. 4: Experimental punching load and ultimate rotation $(V_{punch}\text{-}\psi_{punch})_{exp}$ for 113 considered slabs. Square brackets are literature references.

Figure 4 clearly shows that the punching rotation is inversely proportional to the punching load. Therefore, it is important to understand the geometric and mechanical parameters which influence this phenomenon.

The geometrical and mechanical parameters of the slab database are presented in Table 2. In addition, Figure 5 presents the frequency distribution of the abovementioned parameters, where it can be seen that 75% of the sample exhibits a slenderness ratio h/L=0.10. This value ensures that the slabs flexural behaviour is acceptable and conform to international standards. The distributions of other parameters are approximately uniform. The authors consider the sample to be representative of the typical RC slab population, and suitable for testing the theoretical models presented in the previous section.

Tab. 1 Reference, publication year, number of samples, primary focus of research, and punching rotation assessment method of experimental database.

Ref.	Year	No. of samples	Primary research focus and characteristics.	ψ
[10]	1996	7	High strength concrete; proposal for a new failure criterion.	*I*
[11]	2005	10	Low flexural reinforcement ratio ρ, variations of slabs dimensions and maximum aggregate size. Crack development, comparison between the ACI 318, EC2, and CSCT models.	*D*
[12]	2000	6	Scale effect; comparison between ACI 318 and Canadian standard model.	*I*
[13]	1956	22	CSCT model; investigated parameters: concrete compressive strength f_c; flexural reinforcement ratioρ; compressive reinforcement ratio ρ'; load surface dimensions; and boundary conditions.	*D*
[14]	2016	15	Recycled concrete; concrete compressive strength f_c.	*I*
[15]	2012	6	Recycled concrete; concrete compressive strength f_c.	*I*
[16]	2013	12	Flexural reinforcement ratio ρ.	*I*
[17]	2012	5	Experimental test for validation of Muttoni model.	*D*
[18]	2015	8	Recycled concrete; concrete compressive strength f_c.	*I*
[19]	2015	4	High strength concrete; concrete compressive strength f_c; flexural reinforcement ratio ρ; comparison between ACI 318, EC2, and MC10 models.	*I*
[20]	1996	18	High strength concrete; concrete compressive strength f_c; flexural reinforcement ratio ρ; comparison between ACI 318, EC2, MC90, and BS8110.	*D*

Tab. 2 Variability of geometrical and mechanical parameters of slab database.

Symbol	Parameters	n	x_{min}	x_{max}	$\overline{x}$
h	Thickness (mm)	113	50	550	148
h/L	Thickness/span	113	0.05	0.31	0.09
ρ	Flexural reinforcement ratio	113	0.15%	3.7%	1.1%
ρ'/ρ	Top / bottom reinforcement ratio	56	0.11	1	0.53
a/L	Load surface size/span	113	0.05	0.28	0.13
d_g	Maximum aggregate size (mm)	113	4.0	38.1	18.3
d_g/h	Maximum aggregate size/thickness	113	0.02	0.4	0.16
f_c	Concrete compressive cylindrical strength (MPa)	113	12.8	130	50
f_y	Steel yielding strength (MPa)	113	303	709	504

Please cite this document as: Pani, L., Stochino, F. Punching of reinforced concrete slab without shear reinforcement: Standard models and new proposal. *Front. Struct. Civ. Eng.* (2020). https://doi.org/10.1007/s11709-020-0662-z

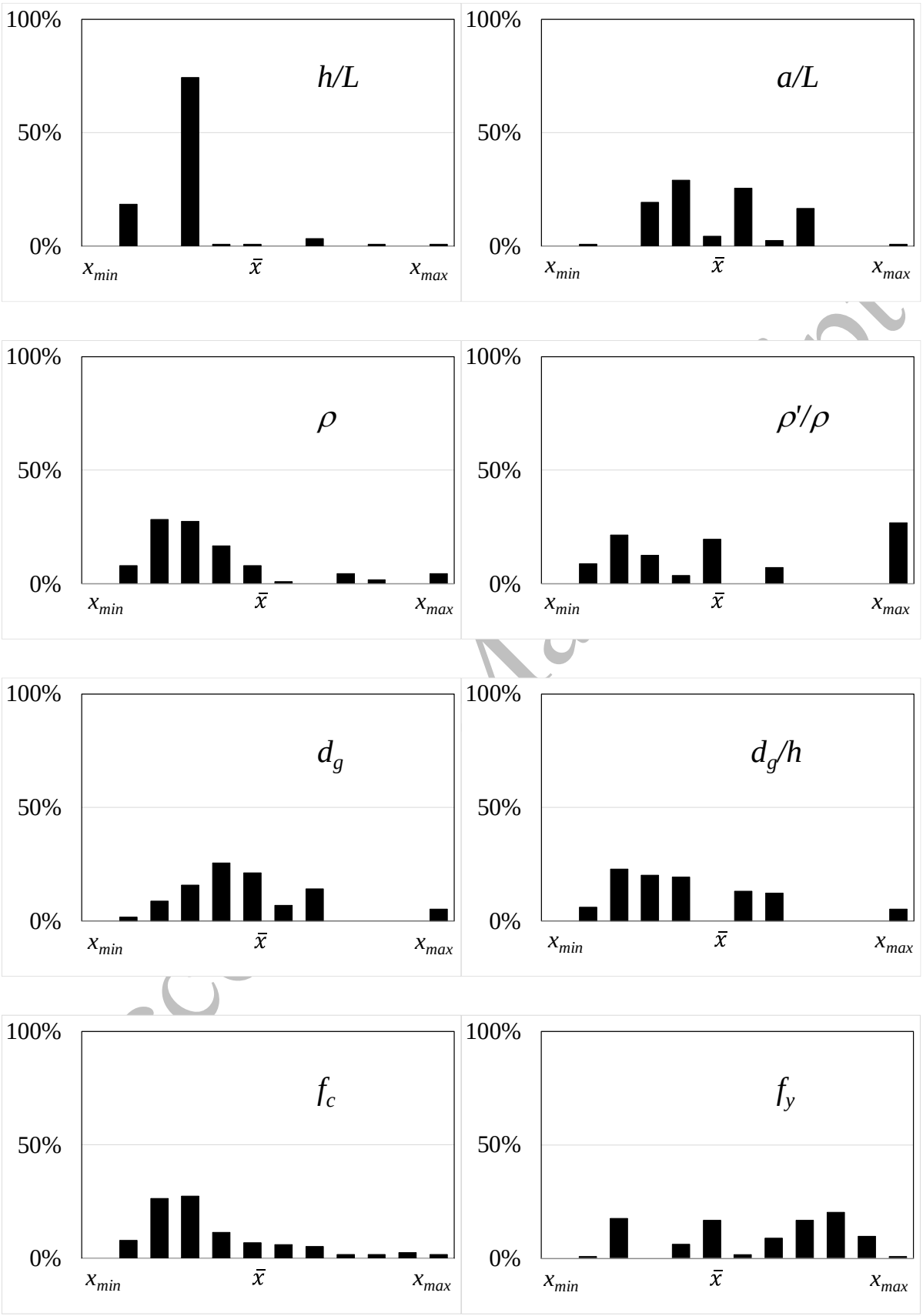

Fig. 5: Frequency distribution of sample mechanical and geometrical parameters.

Please cite this document as: Pani, L., Stochino, F. Punching of reinforced concrete slab without shear reinforcement: Standard models and new proposal. *Front. Struct. Civ. Eng.* (2020). https://doi.org/10.1007/s11709-020-0662-z

Given the high variance of the abovementioned parameters it is essential to consider a dimensionless punching load. In agreement with ACI 318 and MC10, the experimental punching load $V_{punch,exp}$ is transformed into a dimensionless load:

$$V_{punch,exp,adm} = \frac{V_{punch,exp}}{d \cdot b_0 \cdot \sqrt{f_c}} \quad (9)$$

where b_0 is the critical perimeter at a distance $d/2$ from the actual load area. The correlation diagrams between the dimensionless punching load and the other parameters are presented in Figures 6–11. The applicable correlation coefficients r are given in each figure:

$$r = \left| \frac{\sum_i^n (x_i - \bar{x})(y_i - \bar{y})}{\sqrt{\sum_i^n (x_i - \bar{x})^2} \sqrt{\sum_i^n (y_i - \bar{y})^2}} \right| \quad (10)$$

where x_i and y_i are the investigated variables; and $\bar{x}$ and $\bar{y}$ are the average values of the variables, respectively.

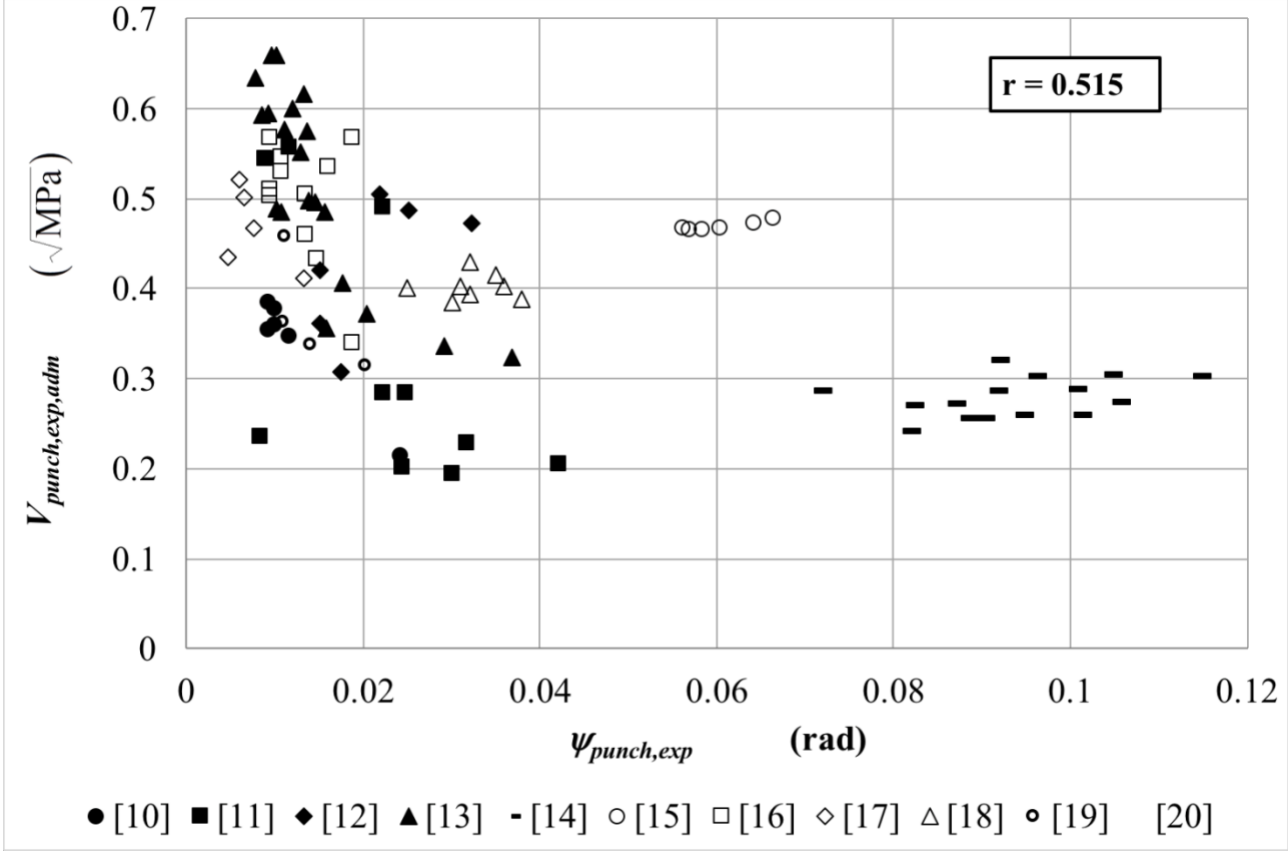

Fig. 6: Comparison of test results: $V_{punch,exp,adm}$-$\psi_{punch,exp}$.

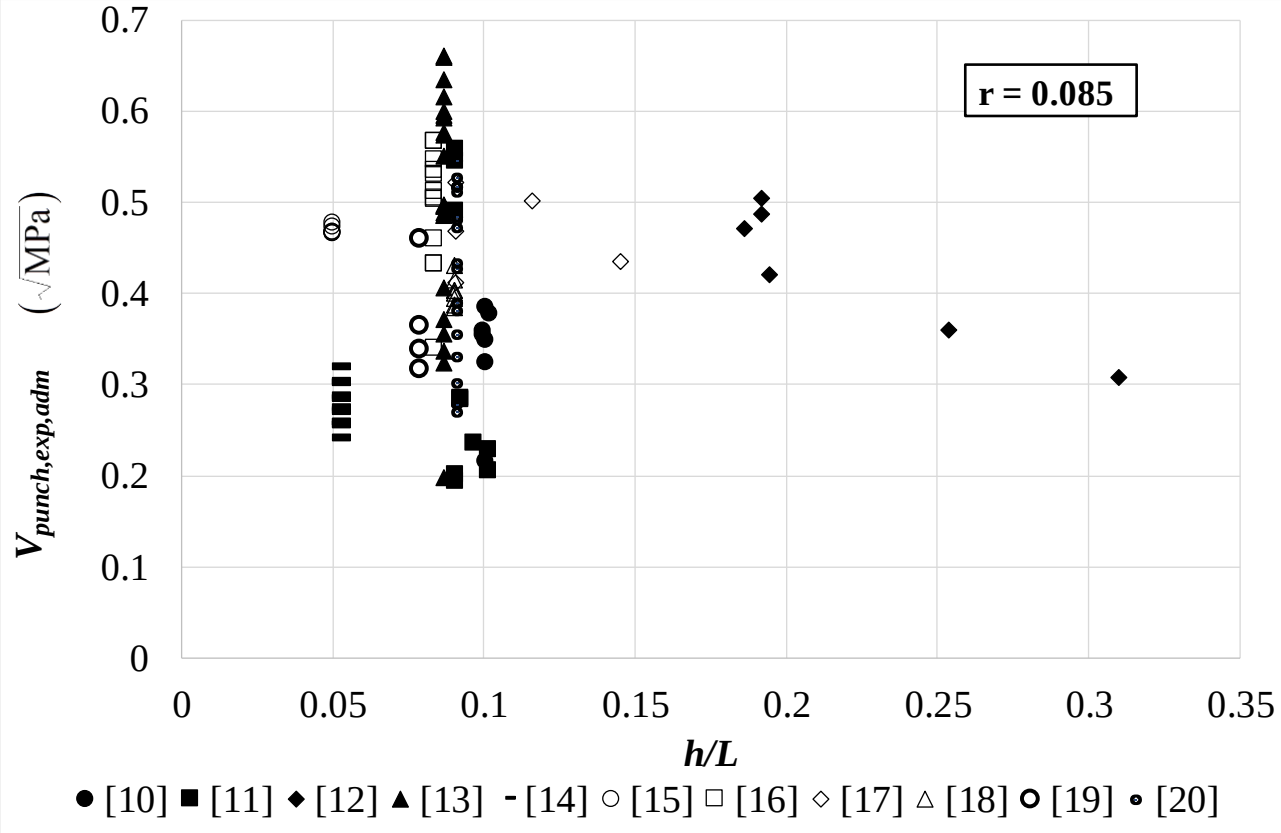

Fig. 7: Comparison of test results: $V_{punch,exp,adm}$-h/L.

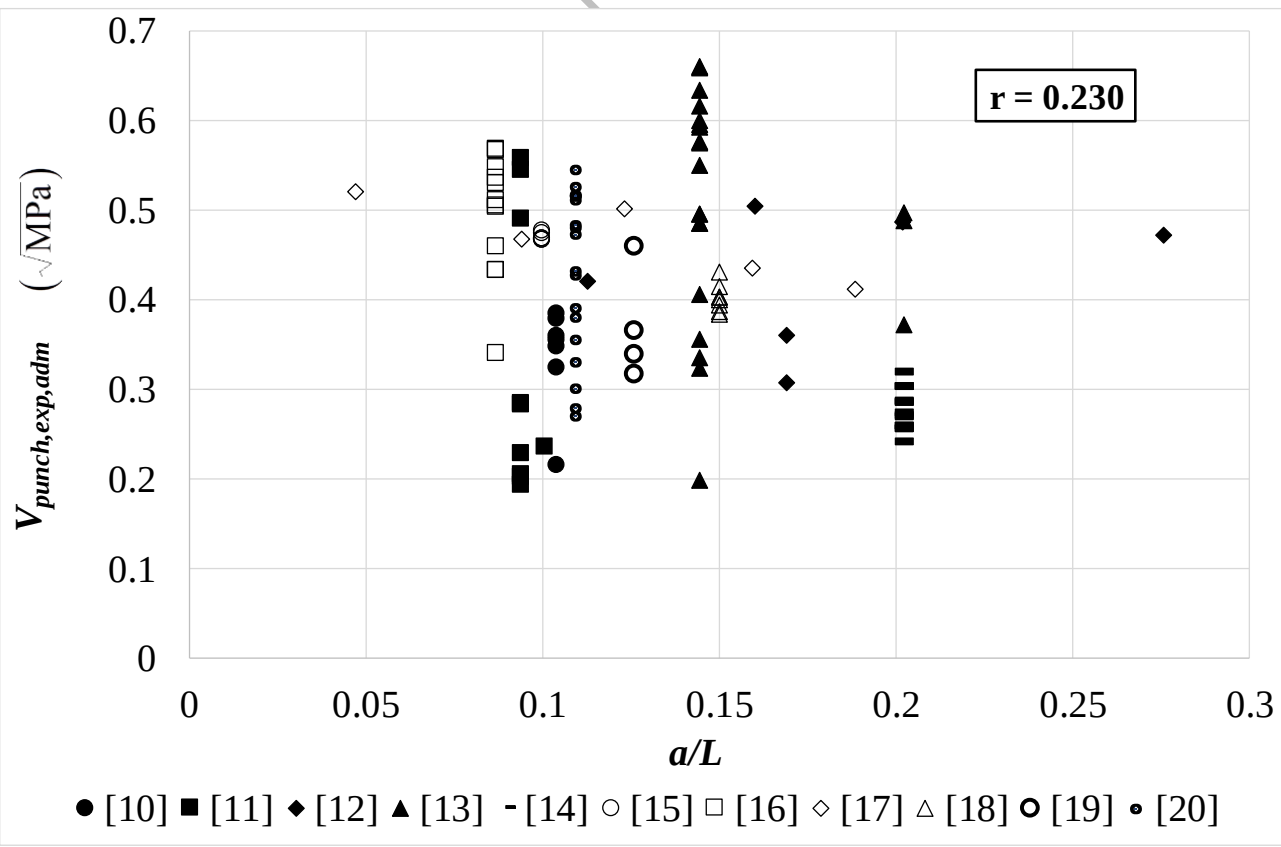

Fig. 8: Comparison of test results: $V_{punch,exp,adm}$-a/L.

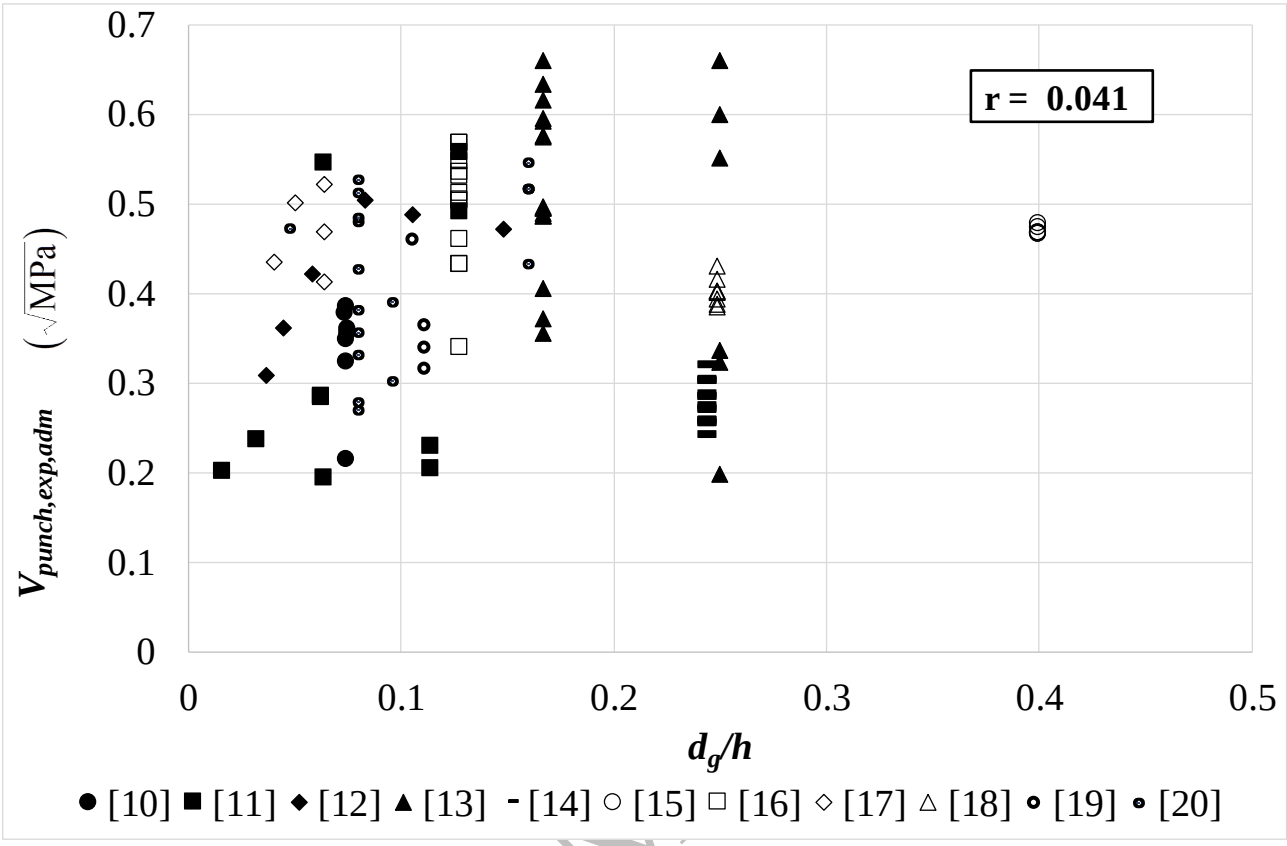

Fig. 9: Comparison of test results: $V_{punch,exp,adm}$-d_g/h.

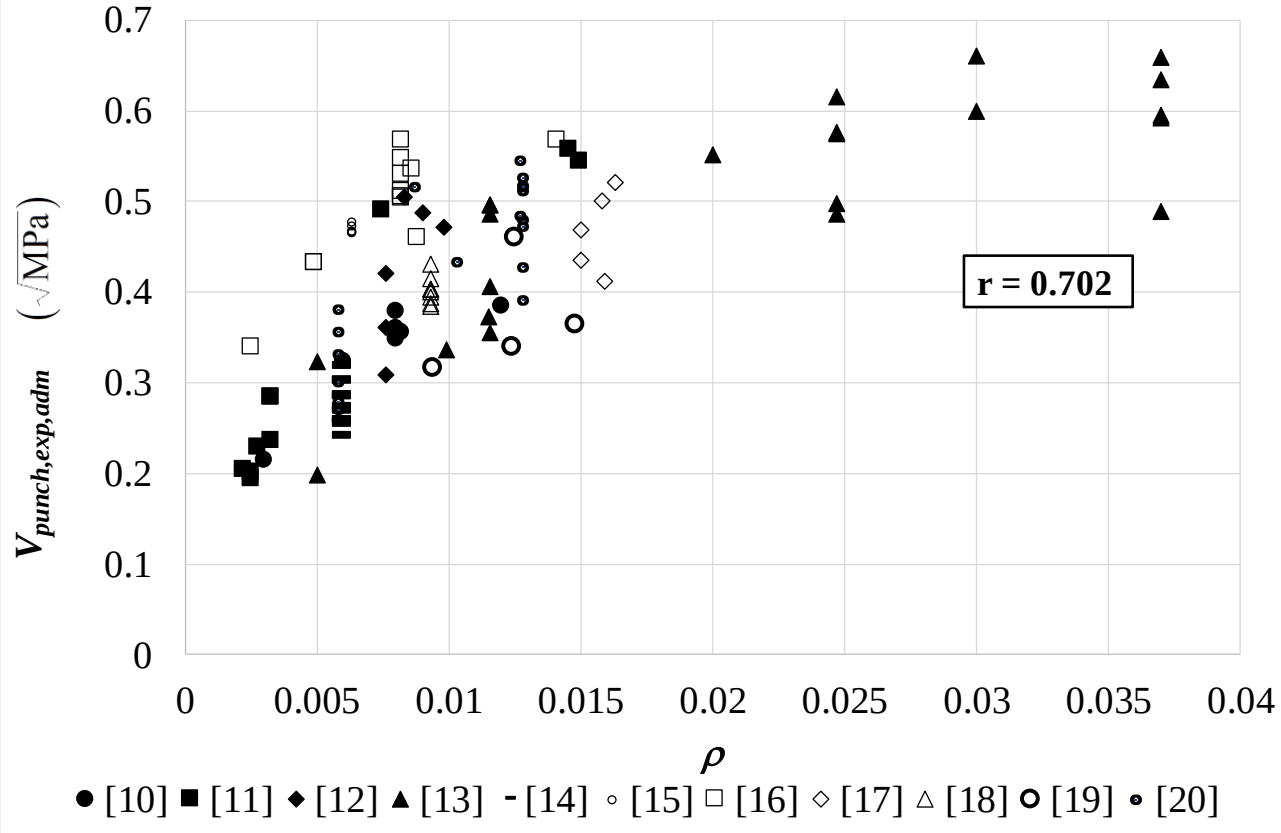

Fig. 10: Comparison of test results: $V_{punch,exp,adm}$-ρ.

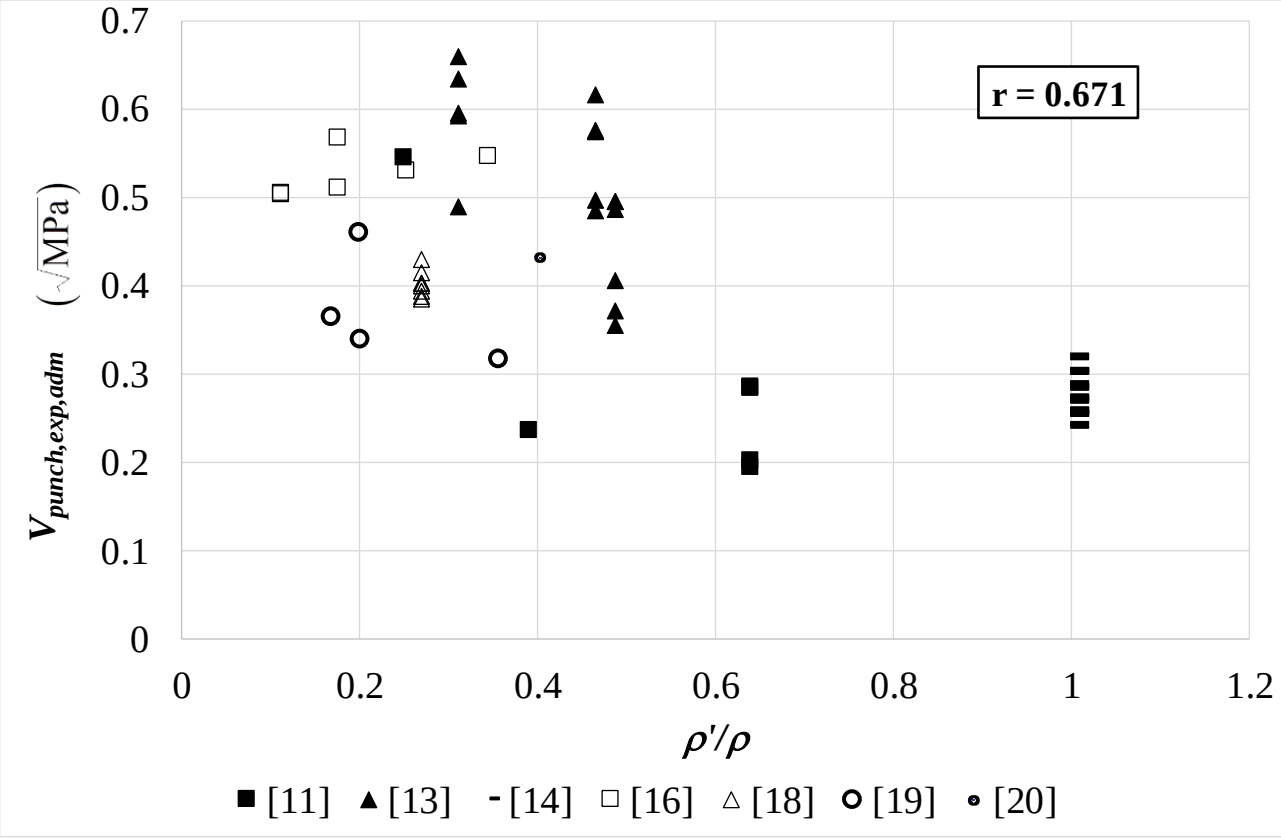

Fig. 11: Comparison of test results: $V_{punch,exp,adm}$-ρ'/ρ.

Figure 6 shows a clear correlation between the dimensionless punching shear strength and the punching rotation. The value of *r* is significant (0.515) and it can be observed that greater values of ψ correspond to smaller load values.

As can be seen in Figure 7, the slenderness correlation is not clear. As discussed previously, the experimental parameter was not investigated across a wide range of this variable, and it is difficult to observe its influence on the punching shear strength.

There is significant variance in the a/L -$V_{punch,exp,adm}$ and $D_{aggr,max}/h$ -$V_{punch,exp,adm}$ correlations, and there is no clear trend in Figures 8 and 9. However, a clear trend can be observed in Figure 10 where the flexural reinforcement ratio has the greatest value of the correlation coefficient *r* (0.702), and it can be concluded that the greater the value of ρ, the greater the punching shear strength. Finally, the ratio between top and bottom reinforcement ratio ρ'/ρ also exhibits a strong correlation with the punching load. In this case the variance is significant, but it is apparent that the greater the ratio, the smaller the punching shear strength.

Figure 12, extracted from [21], presents the load-rotation curves obtained by Kinnunen-Nylander [22]. A strong correlation can be clearly identified between the dimensionless punching load, the rotation ψ, and the flexural reinforcement ratio ρ.

Muttoni [21] reported that the dimensionless punching load $V_{punch,exp,adm}$ and the ultimate rotation $\psi_{punch,exp}$ (Fig. 12, rectangular spots) are highly dependent on the flexural reinforcement ratio ρ. Greater values of $\psi_{punch,exp}$ correspond to smaller values of ρ and $V_{punch,exp,adm}$, and a smaller $\psi_{punch,exp}$ corresponds to greater values of ρ and $V_{punch,exp,adm}$.

The authors developed a database characterised by a greater variation range of the flexural reinforcement ratio ρ, which enabled an expansion of what was reported in [22] and [21]. In Figure 13, it can be seen that for smaller values of flexural reinforcement ($0.50\% < \rho < 0.60\%$) there is a significant data variance. In particular, when ρ is small ($0.20\% < \rho < 0.30\%$), there is a poor correlation between the ultimate

rotation and punching shear strength. However, with mid-sized (0.70% <ρ< 1.20%) and greater (2% <ρ< 4%) values of ρ, the flexural reinforcement ratio trend reported by [22] and [35] is clearly observed.

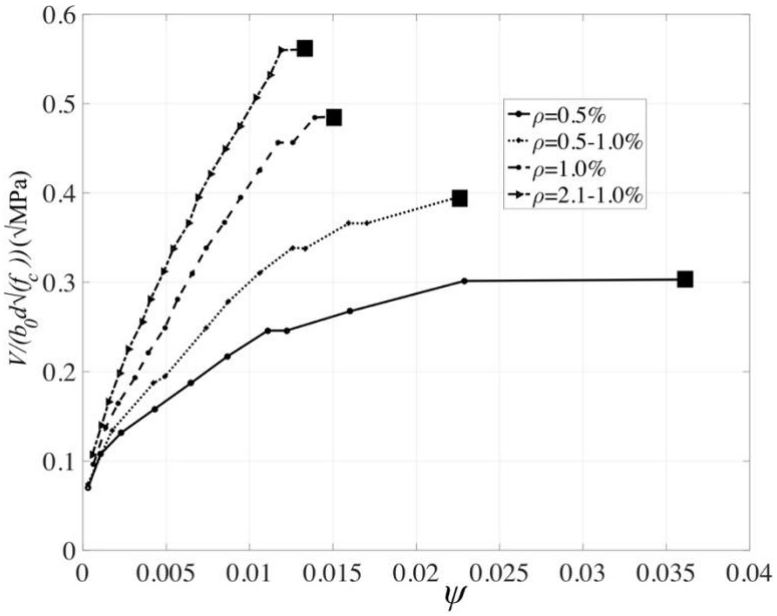

Fig. 12: Load-rotation curves from Kinnun–Nylander tests [22].

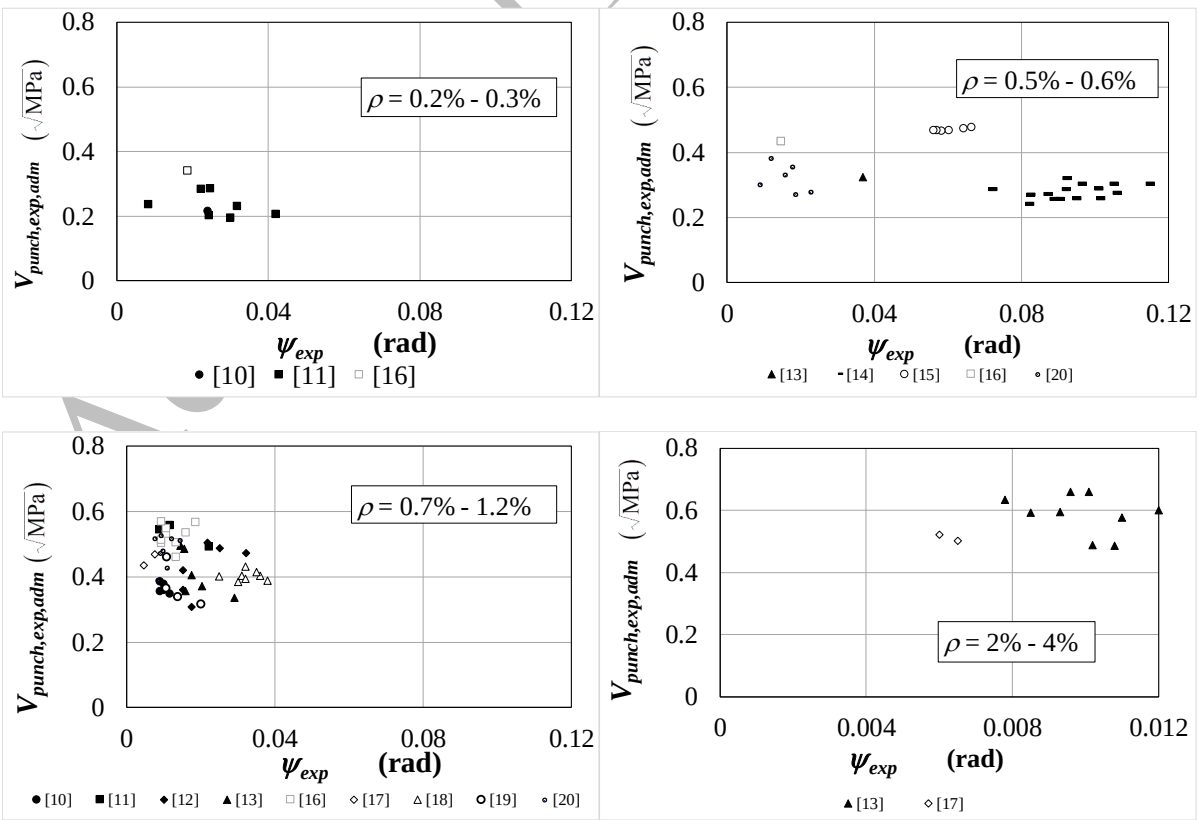

Fig. 13: Comparison of test results: $V_{punch,exp,adm}$-ψ_{exp} for different ρ.

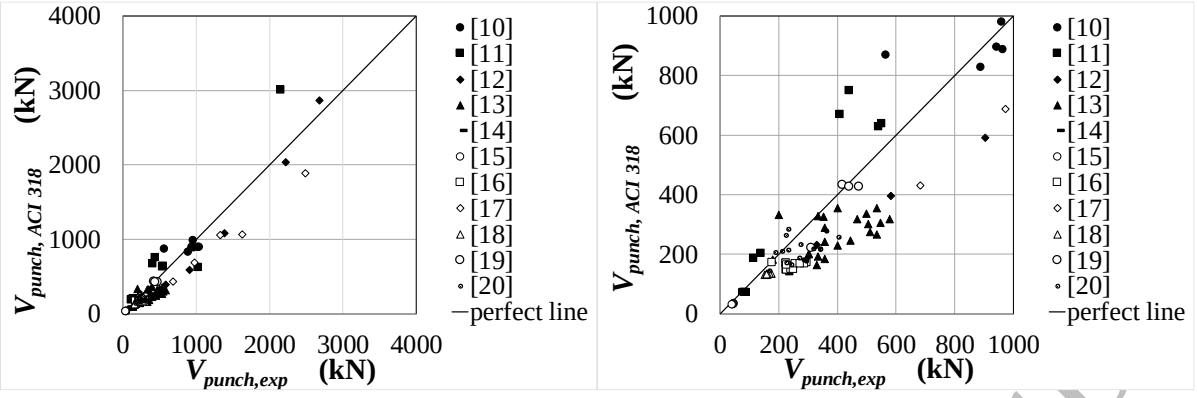

a) b)

Fig. 14: Comparison between experimental and theoretical punching loads obtained using ACI 318 punching model. a) Complete dataset; b) Range 0–1000 kN.

4. International standards models for punching shear strength

4.1 ACI 318 punching model

Figure 14 shows a comparison between the database experimental punching loads $V_{punch,exp}$ and the theoretical values obtained using ACI 318 ($V_{punch,ACI\ 318}$) approach, discussed in Section 2.1. The complete experimental dataset is shown in Figure 14.a, and the range 0–1000 kN is shown in Figure 14.b. The values of $V_{punch,ACI\ 318}$ were estimated using equations (1–3) with $f_c = f_{cm}$.

4.2 Eurocode 2 punching model

The experimental punching loads $V_{punch,exp}$, and the theoretical values obtained using the EC2 model ($V_{punch,EC2}$), discussed in Section 2.2, are shown in Figure 15. The complete experimental dataset is shown in Figure 15.a, and the range 0–1000 kN is shown in Figure 15.b. $V_{punch,EC2}$ was estimated using equation (2) with $\gamma_c = 1$ e $f_{ck} = f_{cm}$.

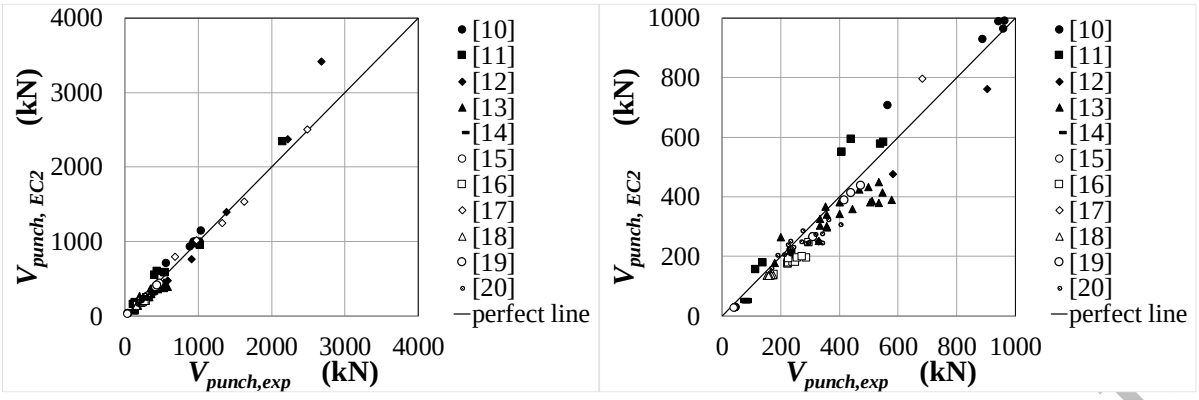

a) b)

Fig. 15: Comparison between experimental and theoretical punching loads obtained using EC2 punching model. a) Complete dataset; b) Detail of range 0–1000 kN.

4.3 Model Code 2010 simplified punching model (level II)

Figure 16 presents a comparison between the experimental punching loads $V_{punch,exp}$ and the theoretical values ($V_{punch,MC10}$) obtained using the simplified MC10 approach presented in Section 2.3. The complete experimental dataset is shown in Figure 16.a, and the range 0–1000 kN is shown in Figure 16.b. The values of $V_{punch,MC10}$ were estimated using equations (5) and (6) with $\gamma_c = 1$ and $f_c = f_{cm}$. This approach is based on an effective bending moment re-distribution. The rotations around the supported area are calculated with level II approximation (see [9] §7.3.5.4).

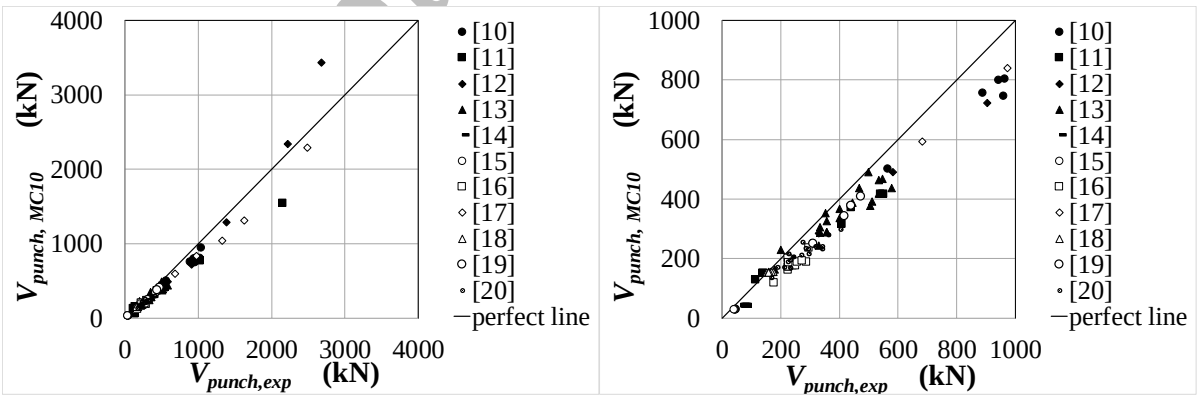

a) b)

Fig. 16: Comparison between experimental and theoretical punching loads obtained using simplified MC10 model. a) Complete dataset; b) Range 0–1000 kN.

Figure 17 shows the comparison between the experimental and theoretical punching rotation ψ_{punch} values. Figure 17.a shows the complete dataset, and Figure 17.b the range 0–0.04 rad.

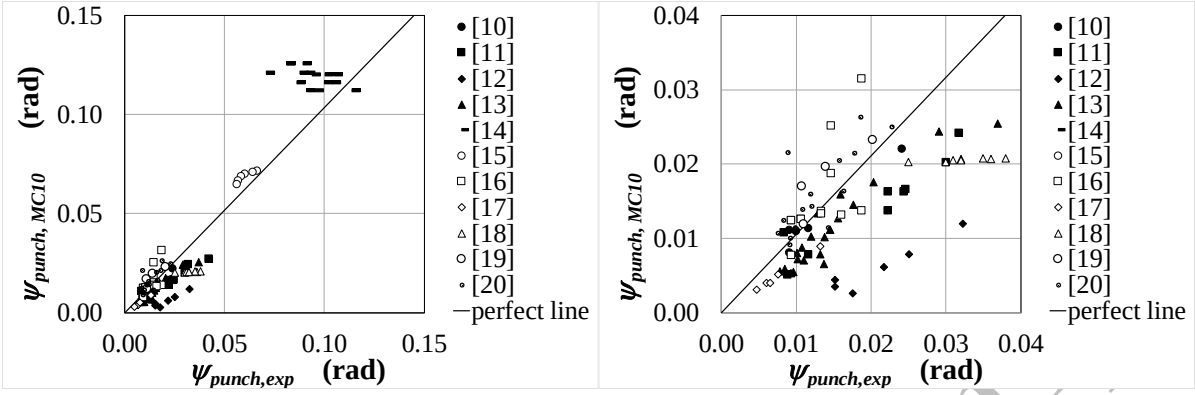

a) b)

Fig. 17: Experimental punching rotation and theoretical values using MC10 model. a) Complete dataset; b) Range 0–0.04 rad.

The MC10, ACI 318, and EC2 punching models were found to be accurate in determining the punching shear load, and the average ratio between the experimental and theoretical values is marginally greater than one in each case. Only the MC10 model could determine the ultimate rotation $\psi_{punch,theo}$.

The average, maximum, and minimum values of the ratio $V_{punch,exp}/V_{punch,theo}$ with the corresponding coefficient of variation (*CoV*, see equation (11)) are presented in Table 3. For the MC10 case the same analysis is presented for the ratio $\psi_{punch,exp}/\psi_{punch,theo}$.

$$CoV = \frac{standard\ deviation}{average\ value} = \frac{\sqrt{\sum_{i=1}^{n}(x_i-\bar{x})^2}}{\bar{x}} \quad (11)$$

where $x_i = \frac{V_{punch,exp}}{V_{punch,theo}}$; and $\bar{x} = \sum_{i=1}^{n}\frac{x_i}{n}$.

Tab. 3 Punching shear strength standard models results

	Model	Average	Min.	Max.	*CoV*
$V_{punch,exp}/V_{punch,theo}$	MC10	1.27	0.78	1.77	0.16

	ACI 318	1.27	0.59	2.00	0.26
	EC2	1.17	0.74	1.71	0.18
$\psi_{punch,exp}/\psi_{punch,theo}$	MC10	1.27	0.41	6.81	0.64

From Table 3 it can be seen that the EC2 model yields the best results for punching load determination. The maximum and average values of the $V_{punch,exp}/V_{punch,theo}$ ratio of the EC2 approach are the closest to one, which indicates that excessive oversizing will not occur. The minimum value of the $V_{punch,exp}/V_{punch,theo}$ ratio is smaller than one for all models, which could result in non-conservative designs. In the case of the EC2 model $(V_{punch,exp}/V_{punch,theo})_{min} = 0.74$ by using equation (2) with $\gamma_c = 1$ and $f_c = f_{cm}$. However, if $\gamma_c = 1.5$ and $f_c = f_{ck}$ had been assumed, the theoretical punching load could have been greater than the experimental one. In this specific case $(V_{punch,exp}/V_{punch,theo})_{min}$ increases from 0.74 to 1.23. Therefore, the former approach ensures a safe design.

The MC10 model is more conservative, as it allows an estimation of the ultimate rotation of the slabs, however, there is a significant data scattering. Actually, the collapse criterion of the MC10 is designed to assess the characteristic punching strength and this can explain its conservative results.

The ACI 318 model could be non-conservative with $(V_{punch,exp}/V_{punch,theo})_{min} = 0.59$. Equations (1), (2), and (3) do not contain safety coefficients, and the use of f_{ck} in place of f_{cm} determines a theoretical punching value greater than the experimental one in a number of cases.

5. New proposal for punching load model

The three models (ACI 318, EC2, and MC10) are currently the predominant models available for punching load assessment. ACI 318 is based on a purely empirical model and does not take into account the contribution of the flexural reinforcement. EC2 model is based on the comb model modified by several experimental parameters.

Empirical or conservative simplified approaches (like those presented in ACI 318 or EC2) can be sufficient for early punching design. But in order to develop a more effective design it is necessary to truly understand the physical phenomena. Fig. 12 clearly shows as higher rotation ψ corresponds to

lower punching strength *V*. Consequently, the correlation between these two parameters seems very important. For this reason, the authors believe that any physical models of punching should consider also the rotation of the slab. The MC10 approach is based on CSCT, takes into account slab rotations capability and presents different levels of approximation. An improved close form formulation of CSCT has been recently proposed by Simões et al. [41]. In the same document the authors state that there is no consensus on the mechanics governing the punching phenomenon.

These considerations and the results presented in Section 4 indicate that there is a need for an improvement in the estimation of punching shear performance of RC slabs without shear reinforcement. In this study the authors propose a model which allows the punching shear strength and the punching rotation to be estimated with a safe and reliable approach.

The assessment of the punching shear strength and the ultimate rotation necessarily implies prior knowledge of the flexural behaviour of the RC slab without shear reinforcement.

To simplify the MC10 approach, the authors propose:

- a new parabolic load-rotation curve based on the CSCT with smaller computational costs; and
- a new failure criterion which takes the correlation analyses into account.

The correlation analysis between the geometrical and mechanical characteristics of the slabs, and the ultimate punching load and rotation (see Figures 6–11), indicate that the flexural reinforcement ratio is a key-parameter with the greatest correlation coefficient $r = 0.702$, as can be seen in Figure 10. On the contrary, the maximum aggregate size does not present significant values of the correlation coefficient, $r = 0.041$. In addition, the compressive reinforcement ratio ρ'/ρ proved to have a relatively significant correlation coefficient, as can be seen in Figure 11. However, this new model does not take the compressive reinforcement ratio into account for three primary reasons:

- the load-rotation curve does not significantly change its shape when considering the compressive reinforcement ρ'. However, the computational costs of a model taking ρ' into account increases, while disregarding its contribution is on the conservative side;
- the slabs with compressive reinforcement in the experimental database are limited (56 out of 113 samples);

- given the geometrical and mechanical characteristics of the considered slabs, the compressive reinforcement can also be in the tensile regime at collapse, which, in conjunction with the abovementioned issues, indicate the complexities when assessing the actual influence of compressive reinforcement on the punching load

Considering these issues, a new failure criterion, based on the MC10 model (see equation (6)), is proposed.

The theoretical punching load $V_{punc,theo}$ and the corresponding ultimate rotation $\psi_{punc,theo}$ can be determined by the intersection between the failure criterion and a simplified load-rotation curve.

5.1 Simplified load-rotation relationship

A parabolic relationship between the punching load and rotation has been assumed on the horizontal axis. This approach is based on the consideration that the experimental V - ψ relationships can be represented by a simple parabolic curve. Its vertex is located at the origin of the reference system and it comprises the limit point ($\psi_{R,flex}$, $V_{R,flex}$), where $V_{R,flex}$ and $\psi_{R,flex}$ can be determined according to equations (A19) and (A20) in Appendix A. The load-rotation and the corresponding rotation-load curve equations are as follows:

$$V = V_{R,flex} \cdot \sqrt{\frac{\psi}{\psi_{R,flex}}} \tag{12}$$

$$\psi = \frac{\psi_{R,flex}}{V_{R,flex}^2} \cdot V^2 \tag{13}$$

5.2 New failure criterion

The new proposal for failure criterion is defined as follows:

$$V_{R,punch} = k_\psi \cdot \frac{\sqrt{f_c}}{\gamma_c} \cdot b_0 \cdot d \tag{14}$$

where the effective depth is d; and b_0 is the critical perimeter located at $d/2$ from the loading surface.

The sensitivity analysis developed in Section 3 highlighted that the flexural reinforcement ratio ρ has a significant influence on the punching strength, while the maximum aggregate size is less correlated.

Therefore, the parameter k_ψ has been expressed as a function of slab rotation ψ, effective depth d, and flexural reinforcement ratio ρ in equation (15). The influence of the maximum aggregate size d_g has been neglected.

$$k_\psi = \frac{\alpha_1 \cdot \rho^2 + \alpha_2 \cdot \rho + \alpha_3}{\beta_1 + \beta_2 \cdot \psi \cdot d} \leq 0.6 \quad (15)$$

where α_1, α_2, α_3, β_1, and β_2 are numerical parameters.

It is critical to emphasise that the intersection point between the simplified load-rotation curve and this failure criterion can be assessed in closed-form. The value of the ultimate rotation can be expressed by the following equation which represents the only real solution of the 3rd order polynomial expression representing the above-mentioned intersection:

$$\psi = \frac{1}{6d}\left(-\frac{4\beta_1}{\beta_2} + \frac{2^{\frac{4}{3}}\beta_1^2}{A} + \frac{2^{\frac{2}{3}}A}{\beta_2^2}\right) \quad (16)$$

$$A = \frac{\psi_{R,flex}}{V_{R,flex}^2}\left(\begin{array}{c} 27\alpha_3 b_0^2\beta_2^2 d^3 f_c + 2\beta_1^3\beta_2^2\frac{V_{R,flex}^2}{\psi_{R,flex}} + 54\alpha_2\alpha_3 b_0^2\beta_2^4 d^3 f_c\rho + 27\alpha_2 b_0^2\beta_2^4 d^3 f_c\rho^2 + \\ 54\alpha_1\alpha_3 b_0^2\beta_2^4 d^3 f_c\rho^2 + \\ 54\alpha_1\alpha_2 b_0^2\beta_2^4 d^3 f_c\rho^3 + 27\alpha_1^2 b_0^2\beta_2^2 d^3 f_c\rho^4 + \\ 3\sqrt{3}b_0 d^{\frac{3}{2}}\left(\beta_2^7 f_c\left(\begin{array}{c} 27\alpha_3 b_0^2\beta_2 d^3 f_c + 4\beta_1^3\frac{V_{R,flex}^2}{\psi_{R,flex}} + \\ 54\alpha_3 b_0^2\beta_2 d^3 f_c\rho(\alpha_2 + \alpha_1\rho) + \\ 27 b_0^2\beta_2 d^3 f_c\rho^2(\alpha_2 + \alpha_1\rho)^2 \end{array}\right)\right)^{\frac{1}{2}} \cdot |\alpha_3 + \rho(\alpha_2 + \alpha_1\rho)| \end{array}\right)^{\frac{1}{3}} \quad (17)$$

The numerical parameters α_1, α_2, α_3, β_1, and β_2 have been tuned using a numerical approach based on the simulated annealing algorithm [42] developed in the MATLAB environment. Using the experimental database, it was possible to tune the failure criterion expressed in equation (14) in order to reduce the difference between the theoretical and experimental values. The values of the unknown parameters were found by minimising $e = \sum_i^{113}\left(\frac{V_{exp}^i - V_{punc,theo}^i}{V_{exp}^i}\right)^2$.

The numerical values of the parameter are:

α_1 = -9997.5787; α_2 = -9988.9091; α_3 = -4005.3062; β_1 = -6937.0915; and β_2 = -1751.8665 (18)

By taking into account the results presented in [11],[36] - [21], and the MC10 [9] approach which considers the influence of the maximum aggregate size d_g on the punching strength, a further definition of k_ψ, also taking d_g into account, is proposed:

$$k_{\psi,dg} = \frac{\delta_1\rho^2+\delta_2\rho+\delta_3}{1.5+0.9k_{dg}\psi d} \leq 0.6 \quad (19)$$

$$k_{dg} = \frac{32}{16+d_g} \geq 0.75 \quad (20)$$

The values of the numerical parameters tuned using the abovementioned numerical approach are as follows:

δ_1 = -181.5905; δ_2 = 8.69371556; δ_3 = 1.12853373 (21)

In this case it is also possible to obtain a closed-form expression for the intersection point between the simplified load rotation curve and this failure criterion:

$$\psi = \frac{5^{\frac{4}{3}}d^2\left(\frac{V_{R,flex}^2}{\psi_{R,flex}}\right)^2 k_{dg}^2 - 10d\frac{V_{R,flex}^2}{\psi_{R,flex}}k_{dg}(C+B)^{\frac{1}{3}} + 5^{\frac{2}{3}}(C+B)^{\frac{2}{3}}}{9d^2\frac{V_{R,flex}^2}{\psi_{R,flex}}k_{dg}^2(C+B)^{\frac{1}{3}}} \quad (22)$$

$$B = 5d^3\left(\frac{V_{R,flex}^2}{\psi_{R,flex}}\right)^3 k_{dg}^3 + 18b_0^2d^6f_c\left(\frac{V_{R,flex}^2}{\psi_{R,flex}}\right)^2 k_{dg}^2\left(\delta_3+\rho(\delta_2+\delta_1\rho)\right)^2 \quad (23)$$

$$C = 6\sqrt{b_0^2d^9f_c\left(\frac{V_{R,flex}^2}{\psi_{R,flex}}\right)^4 k_{dg}^7\left(\delta_3+\rho(\delta_2+\delta_1\rho)\right)^2\left(5\frac{V_{R,flex}^2}{\psi_{R,flex}}+9b_0^2d^3f_ck_{dg}\left(\delta_3+\rho(\delta_2+\delta_1\rho)\right)^2\right)} \quad (24)$$

We now compare the performance of the new proposed model in assessing the punching strength $V_{R,punch\ new\ prop}$ based on the failure criterion characterised by k_ψ (without d_g), and $V_{R,punch\ new\ prop\ with\ dg}$ based on the failure criterion characterised by $k_{\psi,dg}$ (with d_g).

5.3 New model results

Figure 18 presents the load-rotation curves of the MC10 simplified approach and the new proposed model, as well as the above-mentioned failure criteria, the MC10 criterion, and the new failure criterion proposed by the authors (equations (14) and (15)). Three experimental cases were considered when investigating the influence of the flexural reinforcement ratio ρ on the new model effectiveness: small value (ρ = 0.2%) in Figure 18.a [11], average value (ρ = 0.5%) in Figure 18.b [13], and large value (ρ

= 2.5%) in Figure 18.c [13]. The performance of the new model without the contribution of maximum aggregate size is presented in Figures 19 and 20. The theoretical punching load has been obtained from equations (12) and (14) with γ_c = 1 e $f_c = f_{cm}$, and is compared to the experimental value in Figure 19. The theoretical and experimental ultimate rotations are plotted in Figure 20.

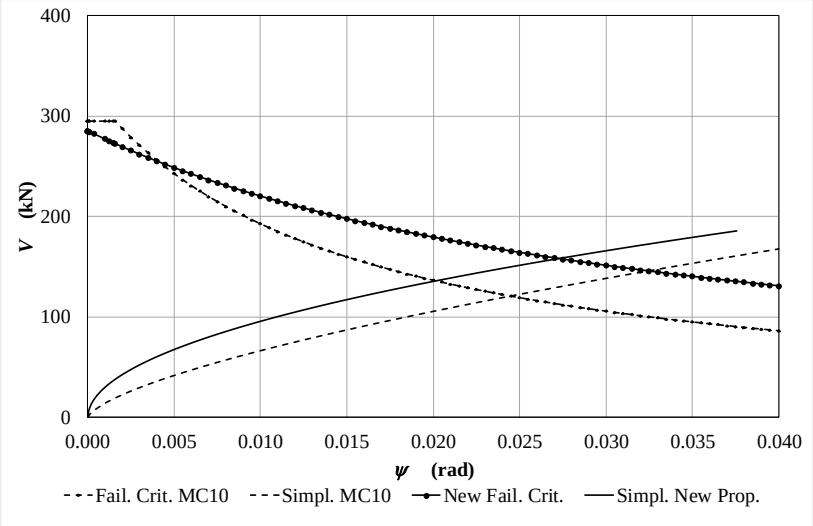

(a) Small value of flexural reinforcement ratio (ρ = 0.2%), case extracted from [11].

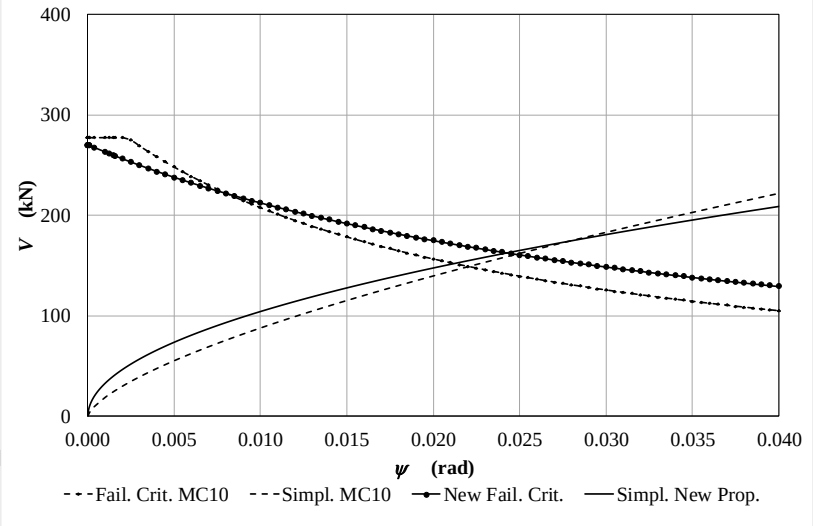

(b) Average value of flexural reinforcement ratio (ρ = 0.5%), case extracted from[13].

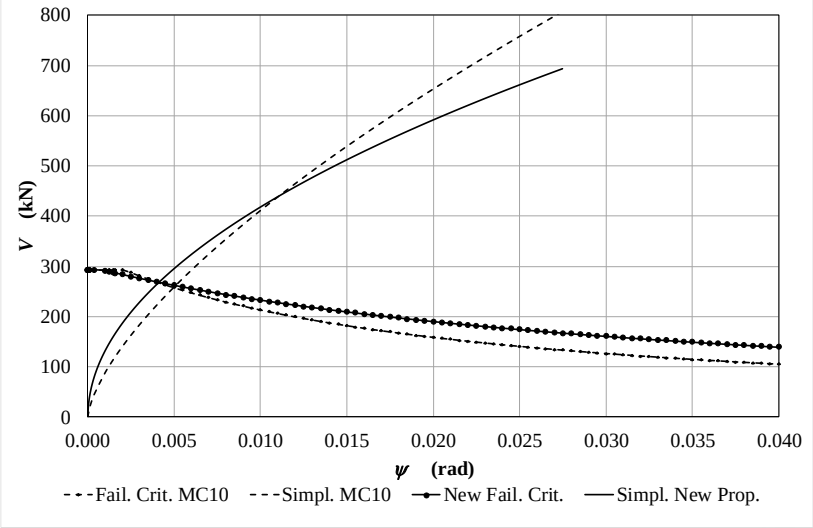

(c) Large value of flexural reinforcement ratio (ρ = 2.5%), case extracted from [13].

Fig. 18: Load-rotation curves and failure criterion of MC10 and proposed approach considering slab tests reported in [11] and [13].

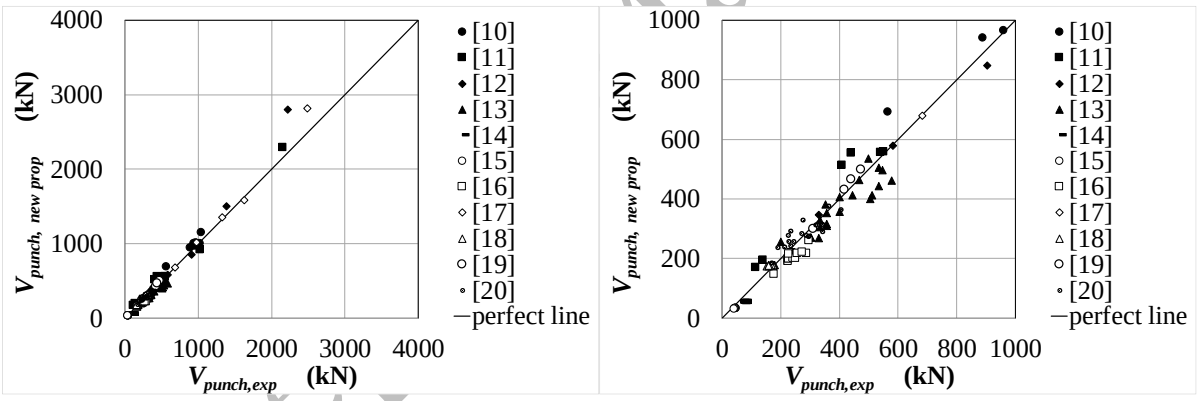

a) b)

Fig. 19: Comparison between experimental and new proposed theoretical punching loads: a) Complete dataset; b) Range 0–1000 kN.

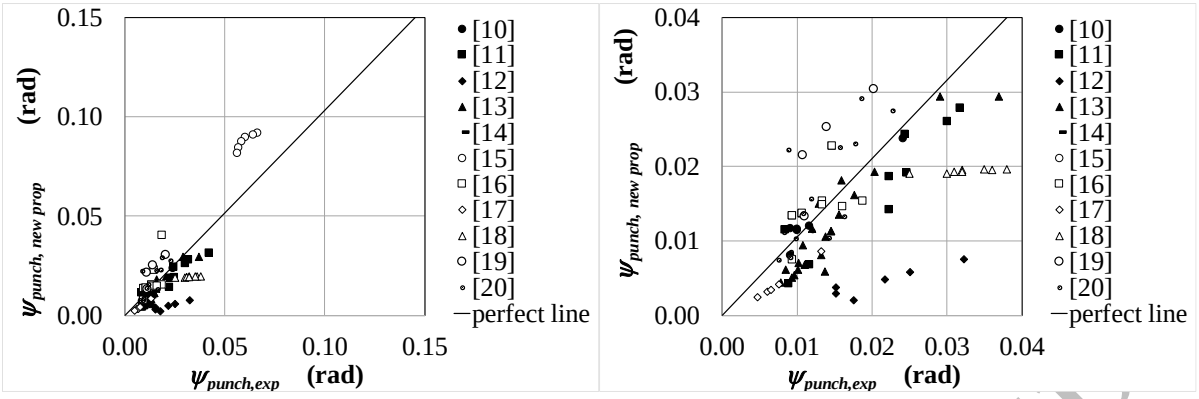

a) b)

Fig. 20: Comparison between experimental and new proposed theoretical ultimate rotation: a) Complete dataset; b) Range 0–0.04 rad.

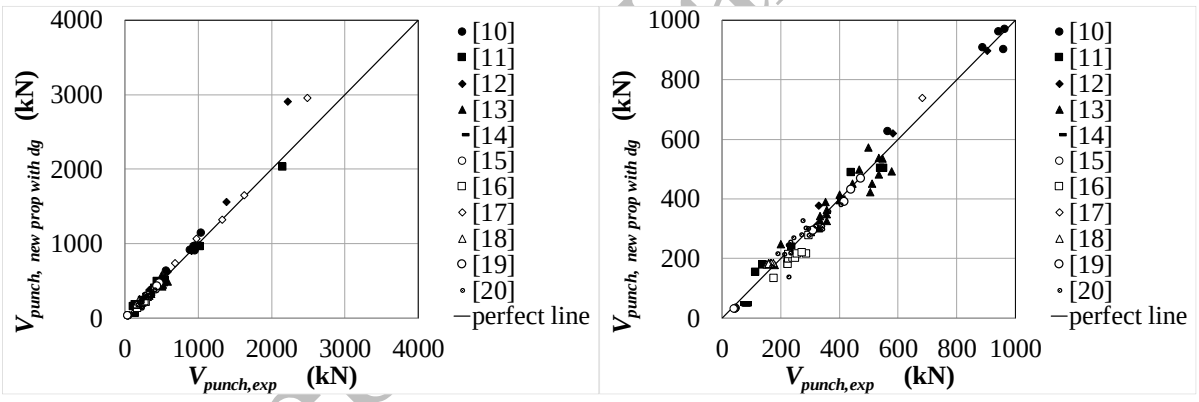

a) b)

Fig. 21: Comparison between experimental and theoretical punching loads obtained using new proposed model with d_g a) Complete dataset; b) Range 0–1000 kN.

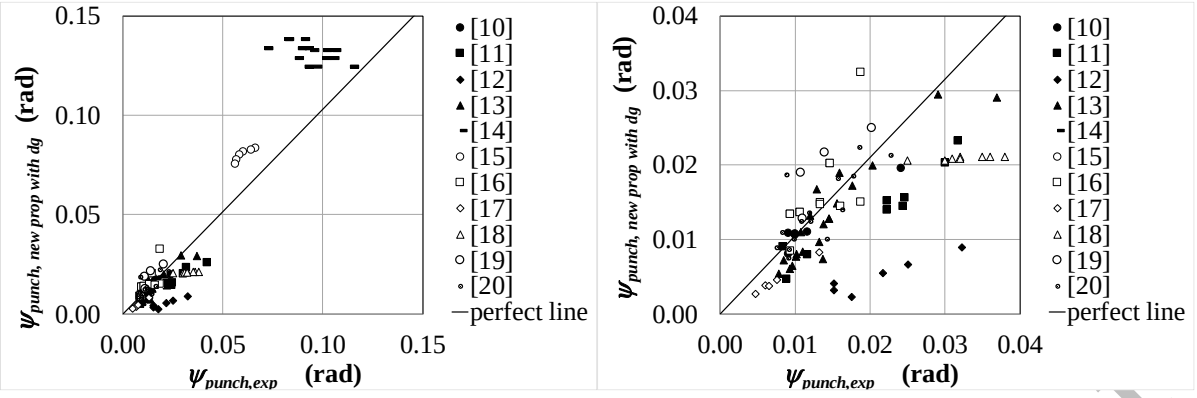

a) b)

Fig. 22: Comparison between experimental and theoretical ultimate rotation obtained using new proposed model with d_g: a) Complete dataset; b) Range 0–0.04 rad.

Figures 21 and 22 present the results obtained with the new proposed model $V_{punch,\ new\ prop\ with\ dg}$ which also takes the maximum size of aggregate d_g into account (equation (19)).

Table 4 presents the average, minimum, and maximum values, as well the *CoV* of the $V_{punch,exp}/V_{punch,theo}$ and $\psi_{punch,exp}/\psi_{punch,theo}$ratios for the new proposed and standards models.

Tab. 4 Models performance in punching load and ultimate rotation estimation.

	Model	**Average**	**Min.**	**Max.**	***CoV***
$V_{punch,exp}/V_{punch,theo}$	MC10	1.27	0.78	1.77	0.16
	ACI 318	1.27	0.59	2.00	0.26
	EC2	1.17	0.74	1.71	0.18
	New proposal	1.06	0.66	1.46	0.16
	New proposal with d_g	1.10	0.62	1.64	0.21
$\psi_{punch,exp}/\psi_{punch,theo}$	MC10	1.27	0.41	6.81	0.64
	New proposal	1.29	0.38	8.68	0.87
	New proposal with d_g	1.27	0.48	7.82	0.75

The failure criterion with the new simplified load rotation curve exhibited highly satisfactory performance. This approach allows the punching performance of RC slabs to be designed in compliance with an advanced and reliable physical model without the need for oversizing. The average value of the $V_{punch,exp}/V_{punch,theo}$ ratio of 1.06 is close to one. From Table 4 it can be seen that the average of the new models is smaller than the 1.17 of the EC2 model. The maximum value of 1.46 of the new proposed models is smaller than the 1.71 of the EC2 model, which ensures a design which limits oversizing. The minimum value of $(V_{punch,exp}/V_{punch,theo})_{min}$ is smaller than the values of the new proposal, which could result in an non-conservative design. This value was obtained assuming $\gamma_c = 1$ e $f_c = f_{cm}$ and using equations (12) and (14). If $\gamma_c = 1.5$ and $f_c = f_{ck}$ had been considered $(V_{punch,exp}/V_{punch,theo})_{min} = 1.1$, which is a safer value. Using the latter parameters, in the case of the EC2 model $(V_{punch,exp}/V_{punch,theo})_{min}$ increased from 0.74 to 1.71. Therefore, it is possible to have a conservative design and, even in this case, to limit the oversizing. The *CoV* is also smaller. The new proposal with d_g exhibited poorer results than the proposed model which neglected the effect of the maximum aggregate size.

With reference to the rotation estimation of slabs (Table 4), the comparison could only be conducted with the simplified MC10 model. The new and MC10 models obtained the same average and minimum values of the ratio $\psi_{punch,exp}/\psi_{punch,theo}$. However, looking at the maximum values there are critical differences, as it is 8.68 for the new model with failure criterion 2, and 6.81 for the MC10 model. This significant difference could signify a different deformation properties estimation which requires further investigation.

However, it is important to highlight that the proposed model is based on the fitting of a quite large, but limited, database. For this reason, its accuracy has been proved only inside this database whose main characteristics are reported in Table 2 and not in every other case. In addition, an accurate study of the ultimate rotation cannot be developed on the basis of the available data, and it can be seen from Table 1 that the rotations were not all evaluated in a similar fashion. In approximately 50% of the cases they were evaluated using a non-direct approach. Therefore, further experimental studies are essential.

Please cite this document as: Pani, L., Stochino, F. Punching of reinforced concrete slab without shear reinforcement: Standard models and new proposal. *Front. Struct. Civ. Eng.* (2020). https://doi.org/10.1007/s11709-020-0662-z

6. Conclusion

In this study an experimental database of 113 RC slabs under punching loads was compiled from data available in the literature. A sensitivity analysis of the parameters involved in the punching strength assessment was conducted, which indicated to the authors the importance of the flexural reinforcement. A new proposal for punching strength and ultimate rotation estimation model for RC slabs was then described. This approach can be seen as a modification of the MC10 simplified model (level II approximation) in the presence of significant redistribution of the bending moment. It is based on a simplified load-rotation curve and on new failure criteria that takes into account flexural reinforcement effects.

The experimental database was used to evaluate the approaches of current international standards, ACI 318, EC2, and MC10, as well as the new proposed model. The latter could be an effective design tool with a relatively simple load-rotation curve definition which would allow the collapse point to be obtained without requiring an iterative process.

Further developments are expected using a computational mechanics approach, similar to those presented in [43] - [46], in order to build a non-linear numerical model tuned on a number of experimental benchmarks capable of improving the sensitivity analysis presented in this study.

In addition, a new experimental campaign was planned by the authors with the aim of improving the literature database. Specifically, the influence of different flexural reinforcement ratio on the punching shear strength and the direct measurement of the slab rotation ψ are the primary aims of future experimental studies.

References

[1] B. Vakhshouri, S. Nejadi, Instantaneous deflection of light-weight concrete slabs. Front. Struct. Civ. Eng 11(4) (2017) 412-423.

[2] J. Wu, X. Liu, Performance of soft-hard-soft (SHS) cement based composite subjected to blast loading with consideration of interface properties, Front. Struct. Civ. Eng., 9(3): (2015) 323-340, DOI: 10.1007/s11709-015-0301-2

[3] J. Baroth, L. Daudeville,, Y. Malécot, Y. About empirical models predicting the missile perforation of concrete barriers, Eur. J. Environ. Civ. En 16(9) (2012), 1074-1089. DOI: 10.1080/19648189.2012.699746

[4] K. Micallef, J. Sagaseta, M.F. Ruiz, A. Muttoni, Assessing punching shear failure in reinforced concrete flat slabs subjected to localised impact loading, Int. J. Impact Eng.71(2014) 17-33. DOI: 10.1016/j.ijimpeng.2014.04.003

[5] J. Sagaseta, N. Ulaeto, J. Russel, Structural robustness of concrete flat slab structures, in Proceedings of ACI-fib International Symposium on Punching Shear of Structural Concrete Slabs 2016; Philadelphia; United States; 25 October 2016, Code 135574.

[6] Fib Bulletin N. 81, Punching shear of structural concrete slabs. Technical Report, 2017

[7] EN-1992-1-1, Eurocode 2 – Design of Concrete Structures. Part 1–1: General Rules and Rules for Buildings, 2008.

[8] ACI 318, Code Requirements for Reinforced Concrete, 2011.

[9] FibBulletin N. 66, Model Code 2010, vol.2.

[10] M. Hallgren, Punching Shear Capacity of Reinforced High Strength Concrete Slabs, doctoral thesis, Royal Institute of Technology, Stockholm, Sweden, 1996.

[11] S.Guandalini, Symmetric Punching in R/C Slabs, doctoral thesis, No. 3380, EPFL, Lausanne, Switzerland, 2005 (in French).

[12] K.K.L. Li, Influence of size on punching shear strength, doctoral thesis, Department of Civil Engineering and Applied Mechanics, McGill University Montreal, Canada, 2000.

[13] R.C.Elstner, E. Hognestad, Shearing Strength of Reinforced Concrete Slabs ACI J. Proc. 53(2) (1956) 29-58.

[14] L. Francesconi, L. Pani, F. Stochino, Punching shear strength of reinforced recycled concrete slabs, Constr. Build. Mat. 127(2016) 248-263. DOI: 10.1016/j.conbuildmat.2016.09.094

[15] H.S. Rao, V.S.K. Reddy, V.G. Ghorpade, Influence of Recycled Coarse Aggregate on Punching Behaviour of Recycled Coarse Aggregate Concrete Slabs, Int. J. Mod. Eng. Res. 2 (4) (2015) 2815–2820. DOI: 10.1.1.416.8390.

Please cite this document as: Pani, L., Stochino, F. Punching of reinforced concrete slab without shear reinforcement: Standard models and new proposal. *Front. Struct. Civ. Eng.* (2020). https://doi.org/10.1007/s11709-020-0662-z

[16] M.F. Ruiz, Y. Mirzaei, A. Muttoni, Post-Punching Behavior of Flat Slabs. ACI Struct. J., 110(5) 2013 801-811.

[17] S. Lips, Punching of Flat Slabs with Large Amounts of Shear Reinforcement, doctoral thesis, No. 5409, EPFL, Lausanne, Switzerland, 2012.

[18] N. Reis, J. de Brito, J.R. Correia, M.R.T. Arruda, Punching behaviour of concrete slabs incorporating coarse recycled concrete aggregates, Eng. Struct. 100 (2015) 238–248, http://dx.doi.org/10.1016/j.engstruct.2015.06.011.

[19] M.M.G. Inácio, A.F.O. Almeida, D.M.V. Faria, V.J.G. Lucio, A. Pinho-Ramos, Punching of high strength concrete flat slabs without shear reinforcement, Eng. Struct. 103 (2015) 275–284, http://dx.doi.org/10.1016/j.engstruct.2015. 09.010.

[20] K.E. Ramdane, Punching shear of high performance concrete slabs 4th International Symposium on Utilization of High-strength/High performance concrete, Paris, 1996 pp.1015-1026.

[21] A. Muttoni, Punching Shear Strength of Reinforced Concrete Slabs without Transverse Reinforcement, ACI Struct. J. 105 (4) (2008) 440-450.

[22] S. Kinnunen, H. Nylander, Punching of Concrete Slabs Without Shear Reinforcement, Transactions of the Royal Institute of Technology, N. 158, Stockholm, Sweden, 1960.

[23] A. Marì, A. Cladera, E. Oller, J.M Bairàn, A punching shear mechanical model for reinforced concrete flat slabs with and without shear reinforcement, Eng. Struct. 166 (2018) 413-426. DOI: 10.1016/j.engstruct.2018.03.079

[24] T.T. Bui, A. Limam, W.S.A. Nana, E. Ferrier, M. Bost, Q.B. Bui, Evaluation of one-way shear behaviour of reinforced concrete slabs: experimental and numerical analysis. Eur. J. Environ. Civ. En. (2017) 1-27. DOI: 10.1080/19648189.2017.1371646

[25] V. Sigrist, E. Bentz, M.F. Ruiz, S. Foster, A.Muttoni,. Background to the fib Model Code 2010 shear provisions–part I: beams and slabs. Struct. Conc., 14(3)(2013) 195-203.

[26] J. Hedebratt, J. Silfwerbrand, Full-scale test of a pile supported steel fibre concrete slab. Mater. Struct., 47 (2014): 647-666, DOI 10.1617/s11527-013-0086-5.

[27] M. Hassan, E.A. Ahmed, B. Benmokrane, Punching-shear design equation for two-way

concrete slabs reinforced with FRP bars and stirrups, Constr. Build. Mat. 66 (2014) 522-532. DOI:10.1016/j.conbuildmat.2014.04.036

[28] M. Bastien-Masse, E. Brühwiler, Experimental investigation on punching resistance of R-UHPFRC–RC composite slabs. Mater. Struct., 49 (2016): 1573-1590, DOI 10.1617/s11527-015-0596-4.

[29] F. Stochino, L. Pani, L. Francesconi, F. Mistretta, Cracking of Reinforced Recycled Concrete Slabs, Int. J. Struct. Glass Adv. Mater. Res. 1(1) (2017) 3-9, DOI: 10.3844/sgamrsp.2017.3.9

[30] M. Etxeberria, A.R. Marí, E. Vázquez, Recycled aggregate concrete as structural material. Mater. Struct., 40(5) (2007): 529-541, DOI: 10.1617/s11527-006-9161-5

[31] J. Xiao, W. Wang, Z. Zhou, M.M. Tawana, Punching shear behavior of recycled aggregate concrete slabs with and without steel fibres. Front. Struct. Civ. Eng., 13(3): 725-740. DOI: 10.1007/s11709-018-0510-6

[32] M. Etxeberria, J.M. Fernandez, J. Limeira Secondary aggregates and seawater employment for sustainable concrete dyke blocks production: Case study, Constr. Build. Mat. 113 (2016) 586-595. DOI: 10.1016/j.conbuildmat.2016.03.097

[33] J.Valivonis, T. Skuturna, M. Daugevičius, A. Šneideris, Punching shear strength of reinforced concrete slabs with plastic void formers, Constr. Build. Mat. 145 (2017) 518-527. DOI: 10.1016/j.conbuildmat.2017.04.057

[34] K.S. Youm, J.J. Kim, J. Moon, Punching shear failure of slab with lightweight aggregate concrete (LWAC) and low reinforcement ratio, Constr. Build. Mat. 65 (2014) 92-102. DOI:10.1016/j.conbuildmat.2014.04.097

[35] M.F.Ruiz, A. Muttoni, J. Sagaseta, Shear strength of concrete members without transverse reinforcement: A mechanical approach to consistently account for size and strain effects, Eng. Struct. 99 (2015) 360-372. DOI: 10.1016/j.engstruct.2015.05.007

[36] J.C. Walraven, Fundamental Analysis of Aggregate Interlock, J. Struct. Eng. ASCE, 107(11) (1981) 2245-2270.

[37] F. J.Vecchio, M.P. Collins, The Modified Compression-Field Theory for Reinforced Concrete

Elements Subjected to Shear, ACIJ. Proc. 83(2) (1986) 219-231.

[38] T.T.Bui, S.Abouri, A.Limam, W.S.A.NaNa, B.Tedoldi, T.Roure, Experiment investigation on shear strength of concrete slabs in nuclear buildings subjected to concentrated loads. Eng. Struct. 131 (2017) 405-420.

[39] W.S.A. Nana, T.T.Bui, A. Limam, S.Abouri,Experimental and Numerical Modelling of Shear Behaviour of Full-scale RC Slabs Under Concentrated Loads, Struct., 10 (2017) 96–116.

[40] W.S.A.Nana, T.T.Bui, M.Bost, A.Limam, Shear Bearing Capacity of RC Slabs Without Shear Reinforcement: Design Codes Comparison, KSCE J. Civ. Eng., (2018) pages 1-14. DOI:10.1007/s12205-018-0612-7

[41] J. T. Simões, M. Fernández Ruiz, A. Muttoni, Validation of the Critical Shear Crack Theory for punching of slabs without transverse reinforcement by means of a refined mechanical model. Struct. Conc., 19(1) 2018 191-216.

[42] S. Kirkpatrick, C.D. Gelatt, M.P. Vecchi, Optimization by simulated annealing, Science220 (4598) (1983) 671-680.

[43] F. Stochino, A. Qinami, M. Kaliske, Eigenerosion for static and dynamic brittle fracture, Eng. Fract. Mech., 182(2017) 537-551. DOI: 10.1016/j.engfracmech.2017.05.025.

[44] F. Buffa, A. Causin, A. Cazzani, S. Poppi, G. Sanna, M. Solci, F. Stochino, E. Turco, The Sardinia Radio Telescope: A comparison between close-range photogrammetry and finite element models Math. Mech. Solids, 22 (5), (2017) 1005-1026. DOI: 10.1177/1081286515616227

[45] Stochino, F., Cazzani, A., Poppi, S., Turco, E. Sardinia radio telescope finite element model updating by means of photogrammetric measurements, Math. Mech. Solids, 22 (4) (2017) 885-901.

[46] G.R. Liu, The smoothed finite element method (S-FEM): A framework for the design of numerical models for desired solutions. Front. Struct. Civ. Eng. 13 (2019) 456. DOI: 10.1007/s11709-019-0519-5

Disclosure Statement

The authors certify that they have no affiliations with or involvement in any organization or entity with any financial interest (such as honoraria; educational grants; participation in speakers' bureaus; membership, employment, consultancies, stock ownership, or other equity interest; and expert testimony or patent-licensing arrangements), or non-financial interest (such as personal or professional relationships, affiliations, knowledge or beliefs) in the subject matter or materials discussed in this manuscript.

Acknowledgement

The financial support of the Autonomous Region of Sardinia under grant PO-FSE 2014–2020, CCI: 2014-IT05SFOP021, through the project "Retrofitting, rehabilitation and requalification of the historical cultural architectural heri- tage (R3-PAS)" is acknowledged by Flavio Stochino.

APPENDIX I – Critical shear crack theory

The critical shear crack theory **(**CSCT) allows the determination of the load-rotation curve which, in the case of an axisymmetric condition, can be obtained by the numerical integration of the moment-curvature relationship. A synthesis of the known CSCT formulation is reported in this section.

The CSCT model identifies a critical inclined crack, whose projection on the extrados surface can be approximated by a circumference of radius r_0 centred at the resultant load application point

. The extrados of the crack portion has a truncated cone shape and is characterised by radial cracks which generate sectors of amplitude $\Delta\varphi$. During collapse, these sectors rigidly rotates describing an angle ψ with respect to the initial horizontal configuration (see Fig. A1). This angle increases with increasing shear load V.

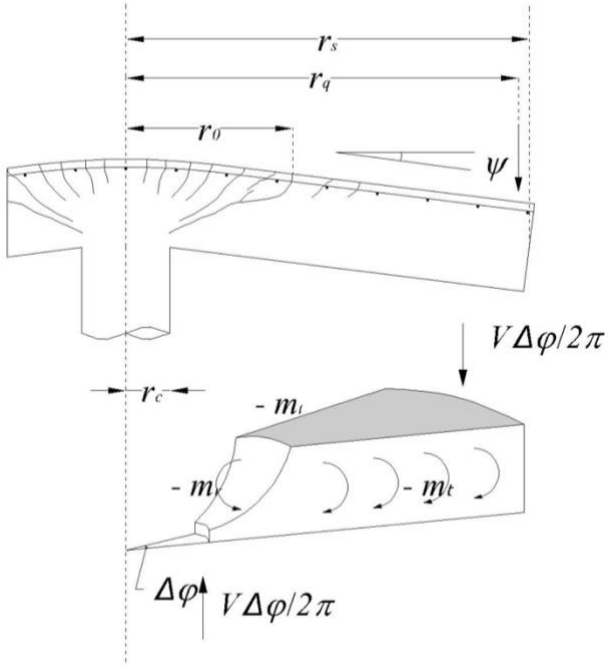

Fig. A1: Kinnunen–Nylander [22] punching model.

The plate can be schematised by a central core delimited by the critical crack and a series of sectors, of amplitude $\Delta\varphi$, delimited by radial cracks. The individual sectors are connected in the compressed area of the slab intrados, close to the loading surface. The inclined component of the load V on the single sector is applied at point O (see Fig A1).

The equation of the rotational equilibrium of the single sector of slab with the pole at point O is as follows (see Fig. A1):

$$V \cdot \frac{\Delta\varphi}{2\pi} \cdot (r_q - r_c) - m_r \cdot \Delta\varphi \cdot r_0 - \Delta\varphi \cdot \int_{r_0}^{r_s} m_t \cdot dr = 0 \qquad \text{(A1)}$$

where r_q is the distance between the reaction of the support and the loading point; and r_c is the radius of the loaded surface.

This model can also represent circular or square plates with uniform or discrete support at the edges, with uniform distribution of reinforcement in both directions.

The radial moment for units of length m_r and the tangential moment for units of length m_t can be expressed as a function of the geometry of the element, the presence of the reinforcement, the

mechanical characteristics of the steel and concrete, and the curvature and rotation ψ produced by the applied load.

The curvature in the tangential direction θ_t, is expressed as a function of rotation ψ:

$$\theta_t = \frac{\psi}{r} \qquad \text{for } r > r_0 \tag{A2}$$

Equation (A2) indicates that tangential curvature θ_t is inversely proportional to the radius.

Inside the critical shear crack the radial and tangential curvature can be considered to be equal:

$$\theta_t = \theta_r = \frac{\psi}{r_0} \qquad \text{for } r \le r_0 \tag{A3}$$

The radius r_0 (see Fig. A1) identifies the position of the circumferential crack, and is equal to (r_c + $d/2$) according to the MC. However, in the Muttoni model [21] $r_0 = r_c + d$, where d is the effective depth of the slab.

The curvature-bending moment relationship can be expressed by a quadrilateral curve:

$$m = E_c \cdot I_0 \cdot \theta \text{ for } \theta \le \theta_{cr} \tag{A4}$$

$$m = m_{cr} \qquad \text{for } \theta_{cr} < \theta \le \theta_1 \tag{A5}$$

$$m = E_c \cdot I_1 \cdot (\theta + \theta_{TS}) \qquad \text{for } \theta_1 \le \theta \le \theta_y \tag{A6}$$

$$m = m_R \qquad \text{for } \theta > \theta_y \tag{A7}$$

The concrete elastic modulus is $E_c = 10000 \cdot \sqrt[3]{f_c}$ (MPa) and its tensile strength is $f_{ct} = 0.3 \cdot \sqrt[3]{f_c^2}$ (MPa). The steel elastic modulus is E_s = 200000 MPa.

The resistant cross section has total height h, effective depth d, and a flexural reinforcement ratio ρ.

For a unitary width b, with an uncracked cross section, it is possible to obtain:

$$I_0 = \frac{h^3}{12} \tag{A8}$$

$$m_{cr} = f_{ct} \cdot \frac{h^2}{6} \tag{A9}$$

$$\theta_{cr} = \frac{m_{cr}}{E_c \cdot I_0} \tag{A10}$$

For a cracked cross section, without compressive reinforcement, using the hypothesis of conservation of the plane sections, perfect adherence of concrete and steel, no traction strength for concrete, and

Hooke's law assumptions, the neutral axis depth x, and moment of inertia I_1 are obtained:

$$x = \frac{E_s}{E_c} \cdot \rho \cdot d \cdot \left(-1 + \sqrt{1 + \frac{2 \cdot E_c}{\rho \cdot E_s}}\right) \quad \text{(A11)}$$

$$I_1 = \frac{x^3}{3} + \frac{E_s}{E_c} \cdot \rho \cdot d \cdot (d - x)^2 \quad \text{(A12)}$$

The contribution of the tensile concrete between two consecutive cracks, tension stiffening, is to be considered constant and produces a reduction of the curvature equal to θ_{TS}:

$$\theta_{TS} = \frac{f_{ct}}{\rho \cdot E_s} \cdot \frac{1}{6 \cdot h} \quad \text{(A13)}$$

Upon reaching the first cracking bending moment m_{cr}, the bending action remains constant while the curvature increases up to the value θ_1:

$$\theta_1 = \frac{m_{cr}}{E_c \cdot I_1} - \theta_{TS} \quad \text{(A14)}$$

The ultimate bending moment m_R is obtained with the following collapse scenario: ultimate compressive strain of concrete equal to 0.00035; yielded reinforcement; stress block for concrete; and ideal elastic-plastic steel as constitutive laws. The presence of compressive reinforcement is disregarded.

$$m_R = \rho \cdot d^2 \cdot f_y \cdot \left(1 - \frac{\rho \cdot f_y}{2 \cdot f_c}\right) \quad \text{(A15)}$$

The yielding curvature θ_y is:

$$\theta_y = \frac{m_R}{E_c \cdot I_1} - \theta_{TS} \quad \text{(A16)}$$

In order to develop equation (A1) it is necessary to use the radial and tangential bending moment ($m_r$and m_t) definitions, as in equations (A4–A7). It is assumed that:

for $r \leq r_0$ $\theta_r = \theta_t = \frac{\psi}{r_0}$ (A17)

for $r > r_0$ $\theta_r = 0$ $\theta_t = \frac{\psi}{r}$ (A18)

The slab failure criterion is satisfied when the circumferential flexural reinforcement, characterised by radius r_s have yielded. In this condition, it is possible, using equation (A1), to calculate $V_{R,flex}$:

$$V_{R,flex} = 2\pi \cdot m_R \cdot \frac{r_s}{(r_q - r_c)} \quad \text{(A19)}$$

By using equation (A18) in the limit condition $r = r_y = r_s \cdot$and$\theta_t = \theta_y \cdot$it is possible to obtain:

$$\psi_{R,flex} = \theta_y \cdot r_s \quad \text{(A20)}$$

In order to obtain the full load-rotation curve it is necessary to develop an iterative process: for the given value of ψ (varying between 0 and $\psi_{R,flex}$), using equation (A1), it is possible to obtain the punching load V using the quadrilateral bending moment-curvature relationship (equations A4–A7)).

Nomenclature

The following symbols are used in this study:

CoV	coefficient of variation
D	direct measurement of ψ
E_c	modulus of elasticity of concrete
E_s	modulus of elasticity of reinforcement
$E_c \cdot I_0$	flexural stiffness before cracking
$E_c \cdot I_1$	flexural stiffness after cracking
I	indirect measurement of ψ
I_0	moment of inertia of concrete gross section
I_1	moment of inertia of reinforced concrete cracked section
L	span of slab
L_x, L_y	span of slab in x- and y-directions, respectively
V	shear force
V_c	concrete contribution to punching shear load
V_{Ed}	shear force from loads
$V_{punch,exp,adm}$	dimensionless experimental punching force
$V_{R,flex}$	shear load capacity
$V_{R,punch}$	punching shear load capacity
$V_{theo,ACI\ 318}$	theoretical punching shear load (ACI 318)
$V_{theo,EC2}$	theoretical punching shear load (EC2)
$V_{theo,MC10}$	theoretical punching shear load (MC10)
$V_{punch,new\ prop}$	new proposed theoretical punching shear load
$V_{punch,new\ prop\ with\ dg}$	new proposed theoretical punching shear load considering aggregate size influence
a	dimension of loaded area of slab
a_x, a_y	column cross section or loaded area dimensions, in x- and y-directions, respectively
b_0	perimeter of critical section

b_x, b_y	cross sectional dimensions, in x- and y-directions, respectively
d	effective depth
d_g	aggregate maximum size
e	optimisation function
f_c	compressive strength of concrete (measured in cylinder)
f_{cm}	average compressive strength of concrete (measured in cylinder)
f_{ck}	characteristic compressive strength of concrete (measured in cylinder)
f_{ct}	tensile strength of concrete
f_y	yield strength of reinforcement
h	depth of slab
k	constant related to size effect of slab
k_1	constant related to prestressing stress
k_{dg}	factor relating to aggregate maximum size
m_{cr}	cracking moment per unit width
m_{Ed}	design bending moment from loads per unit width
m_R	bending moment capacity per unit length
m_{Rd}	design bending moment capacity per unit length
m_r	radial moment per unit width
m_t	tangential moment per unit width
r	general radius or correlation coefficient
r_c	column radius
r_0	radius of the critical shear crack
r_q	radius of load introduction at the perimeter
r_s	radius of isolated slab element
x	depth of neutral axis of reinforced concrete section
x_i	general parameter
$\bar{x}$	average value of general parameter

x_{max}	maximum value of general parameter
x_{min}	minimum value of general parameter
y_i	general parameter
$\bar{y}$	average value of general parameter
$\Delta\varphi$	angle of a slab sector
α_s	constant related to column location in structure
α_1, α_2, α_3	factors accounting for flexural reinforcement ratio
β	ratio between maximum and minimum dimension of column cross section
β_1, β_2	factors accounting for rotation and effective depth
γ_c	partial safety factor for concrete
λ	factor accounting for concrete weight
ρ	flexural (bottom) reinforcement ratio
ρ'	flexural (top) reinforcement ratio
ρ_l	average flexural reinforcement ratio in x- and y-directions
ρ_{lx}, ρ_{ly}	flexural reinforcement ratio in x- and y-directions, respectively
ν_{min}	factor related to size effect of slab and compressive strength of concrete
σ_{cp}	prestressing stress
θ	general curvature
θ_1	curvature in stabilised cracking
θ_{cr}	curvature at cracking
θ_r	curvature in radial direction
θ_t	curvature in tangential direction
θ_{TS}	decrease in curvature from tension stiffening
θ_y	yielding curvature
ψ	rotation of slab outside the column region
$\psi_{punch,exp}$	experimental punching rotation of slab

$\psi_{punch,theo}$ theoretical punching rotation of slab

$\psi_{R,flex}$ capacity of flexural rotation of slab

$\psi_{theo,MC10}$ theoretical punching rotation of slab (MC10)

$\psi_{punch,new\ prop}$ new proposed theoretical punching rotation of slab

$\psi_{punch,new\ prop\ with\ dg}$ new proposed theoretical punching rotation of slab considering aggregate size influence